

博士論文

Development of a semiquantitative analysis
of the complementarity between molecular surfaces
in supramolecular complexes

(超分子会合体における分子表面間の相補性の
半定量的解析法の開発)

田中 成

Contents

Chapter 1. General Introduction	3
1.1. Biological phenomena and chemistry.....	3
1.2. Molecular recognition.....	4
1.3. Intermolecular interactions	5
1.3.1. Direct interaction: van der Waals interaction and exchange repulsion	6
1.3.2. Indirect interaction: the hydrophobic Effect	8
1.4. Construction of supramolecular structures by van der Waals force and the hydrophobic effect	9
1.4.1. Difficulties and meanings of supramolecular assembly by van der Waals interaction and the hydrophobic effect	9
1.4.2. Nanocube: an exceptional example.....	11
1.5. Prediction of affinity.....	16
1.5.1. Importance of contact surface areas.....	16
1.5.2. Importance of intersurface distance	17
1.6. Aim of the thesis.....	18
Chapter 2. Development of Surface Analysis with Various Probe Radius (SAVPR) Method	21
2.1. Three types of molecular surface.....	21
2.1.1. van der Waals surface	21
2.1.2. Connolly surface	21
2.1.3. Solvent accessible surface	22
2.2. Surface Analysis with Various Probe Radius (SAVPR) method	23
2.2.1. Concept.....	23
2.2.2. Formulation	23
2.2.3. Features	26

Chapter 3. Effect of Intersurface Distance Density on Association Affinity	28
3.1. Introduction.....	28
3.2. Analysis of contact surface areas of nanocubes	29
3.3. Analysis of intersurface distance.....	31
3.3.1. Nanocubes in aqueous methanol	31
3.3.2. Nanocubes in pure water	31
3.3.3. Host-guest systems.....	32
3.4. Conclusion	34
3.5. Detailed methods.....	34
Chapter 4. Effect of Small Structural Difference on Self-Assembly	53
4.1. Introduction.....	53
4.2. Structural consideration: possible isomers of the nanocube	54
4.3. Results and discussions	56
4.3.1. Synthesis of the monomer molecule	56
4.3.2. NMR measurements: titration experiments	57
4.3.3. NMR measurements: DOSY experiments.....	59
4.3.4. NMR measurements: variable temperature experiments.....	59
4.3.5. Isothermal titration calorimetry.....	61
4.3.6. MM calculation: optimized structures and their energies	62
4.3.7. SAVPR analysis: intersurface distance distributions	63
4.4. Conclusions.....	64
4.5. Experimental procedures.....	65
Chapter 5. General Conclusion and Prospects.....	71
5.1. General conclusion	71
5.2. Prospects.....	72
Acknowledgements	73

Chapter 1.

General Introduction

1.1. Biological phenomena and chemistry

For a long time, the organisms had been recognized as different existence from the other objects. Such an idea may have stemmed because the organisms have quite special characteristics, for example, spontaneous and complex moves and self-reproduction. However, it is nowadays believed that the organisms and their components obey the same rules of physics as the other normal objects. Their motion is controlled by Newton dynamics and their metabolism is governed by the principles of chemistry. In particular, organic substances, a component of organisms, have essentially nothing special compared with inorganic substances. This fact has been shown by many researches such as Wöhler's experiment where inorganic substances were converted into urea, an organic substance.^[1]

Although the rules that organisms obey are not regarded as a mystery anymore, their mechanisms and regulations are still so sophisticated and elaborate that our science has not perfectly succeeded in understanding the total system or reproducing them. For example, heredity, the resemblance of family members, is now understood as transmission of molecules that possess genetic information from parents to children. The first cell of a child includes molecules that possess genetic information on parents, and this information is replicated when the cells divide. Based on this information, translation, or protein synthesis, is conducted and the body structure of the child is formed. The mechanisms of replication of genetic information and translation from the information to protein structure have already been understood at the molecular level to some extent. However, it is not totally understood whether each character of individuals is inherited. Reproduction of a system also seems to have a long way to go. Replication and translation of genetic information are realized in biological systems by recognition of very subtle difference of molecules and proofreading of mismatched molecules. Although these processes are required to ensure the accuracy of information, they are so sophisticated that they have not been imitated artificially.

As seen in this example, one of the most sophisticated mechanisms of the control of biological chemical reactions is molecular recognition. Next section describes this phenomenon.

1.2. Molecular recognition

Molecular recognition is a phenomenon where a particular molecule is selectively complexed with or captured by other species. Molecular recognition plays a very important role in many biological phenomena.

One of the most typical examples is the complementary base pairing of DNA/RNA. In DNA or RNA, guanine and cytosine are always paired and never paired with other bases. In other words, guanine and cytosine recognizes each other. The same discussion holds for adenine and thymine (or uracil in RNA). These recognitions play an essential role in the replication of DNA/RNA and translation from gene to protein.

Another example is ion channel of cell membrane. Ion channels, regulating the concentration of alkali metal ions such as K^+ and Na^+ , are indispensable to cell activity. This regulation requires the recognition of alkali metal ions. For example, K^+ can pass potassium channels whereas Na^+ and Rb^+ cannot. The exclusion of larger ions from the channel is intuitive. On the other hand, the exclusion of smaller ions is somewhat counterintuitive because they seem to have no steric hindrance. This phenomenon can be understood by considering a very simplified chemical reaction:



For metal ions to enter a channel, they should be dehydrated. On the interior wall of the channel, some oxygen atoms exist and can coordinate to the incoming ions. In a potassium channel, the positions of the oxygen atoms are optimized to coordinate to K^+ ions. This configuration stabilizes the intermediate of the reaction, the $K^+ \subset \text{channel}$ complex. This stabilization cannot sufficiently work for Na^+ . The absence of stabilization means that Na^+ ions are very destabilized in a potassium channel compared with the outer space where Na^+ ions are hydrated. The destabilization of the intermediate slows down the reaction and prevents the pass of Na^+ ions. In this process, molecular recognition determines the stability of intermediate state, drives the selective passage of alkali metal ions through the cell membrane, and keeps the normal cell activities.

Another example of molecular recognition is the bindings of enzyme-substrate and antibody-antigen. These hosts specifically bind the counterpart guests. These molecular

recognitions are enabled by complementary design of host and guest molecules, such as the configuration of hydrogen bond donor/acceptor and the shapes and sizes of molecules. Larger guests than the pocket of host cannot be bound because of steric hindrance. The binding of smaller guests is suppressed by weaker intermolecular interactions. As a result, a guest with matched shape and size is selectively bound to its counterpart.

As can be seen from the abovementioned examples, molecular recognition is driven mainly by intermolecular interactions. Intermolecular interactions determine the affinity of host-guest pairs and, therefore, whether molecular recognition occurs. The comprehensive understanding of molecular recognition will require wide and deep knowledge of intermolecular recognition. The detail of intermolecular interactions is described in the following section.

1.3. Intermolecular interactions

In the process of molecular recognition, many intermolecular interactions are employed, such as electrostatic interaction, hydrogen bond, and van der Waals force. Electrostatic interaction refers to classical electromagnetic attraction/repulsion between charged particles. Hydrogen bond is attractive interaction between a hydrogen atom with partially positive charge and an electronegative atom, where both of electrostatic interaction and orbital interaction contribute. Van der Waals force is a sum of weak interactions other than abovementioned interaction, such as attractive interaction between induced dipoles (London dispersion interaction). This dispersion interaction is universal and exists between any pair of molecules. Another important universal interaction is exchange repulsion, repulsive interaction between electron pairs deriving from the Pauli rule.

When these intermolecular interactions drive an association behavior of molecules, they exert attractive force between the components in the associated complex. In other words, they directly stabilize the complex.

However, without the direct stabilization of the associated complex, the association behavior can still be driven by intermolecular interaction. In the simplest case, the association reaction can be written as:



On the other hand, when the reaction takes place in solution, the reaction equation should be:



where **S** refers to a solvent molecule. If solvent molecules complexed with **A** or **B** are destabilized, or if bulk solvent molecules are largely stabilized, the reaction becomes favored without attractive interaction between **A** and **B**. This phenomenon can be seen as an apparent interaction between **A** and **B** that is present only in solution. This phenomenon is referred to as the solvophobic effect, or especially the hydrophobic effect when the solvent is water. The hydrophobic effect is much more important than other the solvophobic effect because the attractive interaction of hydrogen bond between water molecules is enormously strong.

In this section, weak intermolecular interactions among the abovementioned interactions are described in more detail. Two of them, van der Waals force and exchange repulsion are direct interaction, whereas the hydrophobic effect is indirect interaction.

1.3.1. Direct interaction: van der Waals interaction and exchange repulsion

One of direct weak interactions of great importance is van der Waals force. As mentioned above, van der Waals force is a sum of relatively weak intermolecular interactions. This interaction includes the following contributions:

- dipole-dipole
- dipole-induced dipole
- induced dipole-induced dipole

A molecule without charge or permanent dipole moment can possess a transient dipole moment caused by other charge and an instantaneous dipole moment caused by fluctuation of the density of electrons. This dipole is referred to as an induced dipole. Between a dipole and an induced dipole generated by it, an attractive interaction can occur. This interaction, dipole-induced dipole interaction, is intuitive and an important example of van der Waals force.

Even if two species do not have any multipole (for example, noble gas), an attractive interaction, referred to as London dispersion, still exists between them.^[2] Without such an interaction, noble gases would not condense at low temperature. In a conventional explanation, London dispersion is explained as the attraction between two induced dipoles. Fluctuation of the electron density polarizes a molecule. This polarization means that the molecule becomes an instantaneous induced dipole, which can polarize another molecule. These two polarized

molecules attract each other. When the distance between the molecules is R , the electric field generated by the first dipole has intensity proportional to R^{-3} at the point of another molecule. The dipole moment of the second molecule is proportional to the intensity of the electric field at the point, so proportional to R^{-3} . The interaction energy between them is the product of the electric field and the dipole moment, and therefore proportional to R^{-6} .

Exchange repulsion is another important interaction. This interaction arises from the Pauli rule. This repulsive interaction should be proportional to the overlap of two wave functions. Because the wave functions decay exponentially, the overlap should also decay exponentially. Therefore, this repulsion is very weak when two molecules are sufficiently distant, whereas it becomes large very rapidly as the distance decreases.

These two direct weak interactions are often considered together. When molecules do not possess any multipole, the whole formulation of direct weak interactions should be

$$U(R) = -AR^{-6} + Be^{-CR}$$

where R is the distance between the molecules, $U(R)$ is the potential energy of the molecules, and A , B , and C are positive constants. For convenience of calculation, the repulsion term is often approximated by the negative power of R :

$$U(R) = -AR^{-6} + BR^{-n}$$

Typically, $n = 12$ is adopted while other values such as $n = 9$ are sometimes employed. This type of formulation of intermolecular potential is referred to as Lennard-Jones potential, especially when $n = 12$ (Figure 1-1). Lennard-Jones potential is widely used in molecular simulation.

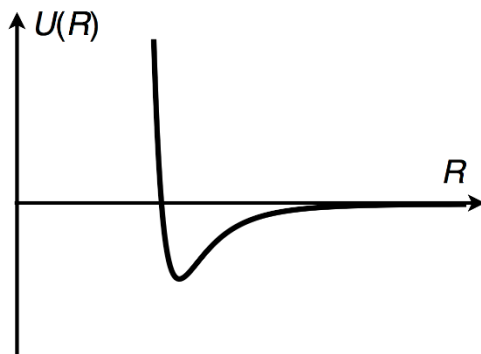


Figure 1-1. Lennard-Jones potential with $n = 12$.

Unlike electrostatic interaction, these direct interactions are a short-range interaction; these interactions rapidly decay at a distant point. In other words, direct interactions have a strong dependency on the intermolecular distance. This point is important to discuss the contribution of direct interactions to an association affinity. Such discussions are presented in the following sections and chapters.

1.3.2. Indirect interaction: the hydrophobic Effect

The hydrophobic effect is a phenomenon where some molecules or moieties of molecules are excluded from bulk water and aggregate because of their low affinity to water. In particular, this phenomenon is often observed when nonpolar or poorly polar molecules are dissolved in water, resulting in aggregation of the molecules. Although the hydrophobic effect is very important and ubiquitous phenomena in natural systems, the full understanding of the hydrophobic effect has not been established. Some origins are considered to contribute to the hydrophobic effect: the structure formation of water molecules around molecular surface, the number of hydrogen bonds of water molecules, and the difference of polarizability between water and solutes.

Classically, the hydrophobic effect is attributed to the structure formation of water molecules around the surface of solute molecules. This structure confines the configuration of the water molecules, thereby decreasing the entropy of the water molecules. Smaller surface areas of solute molecules require the smaller number of water molecules to form the structure, recovering the entropy of the water molecules and decreasing total Gibbs energy in the system. This mechanism drives the minimization of molecular surface, i.e., the hydrophobic effect. This scenario is referred to as “iceberg model” and maintains that the hydrophobic effect is entropy-driven.^[3]

While the hydrophobic effect can be explained by iceberg model in some cases, this is not always true. Actually, the enthalpy-driven hydrophobic effect, referred to as the non-classical hydrophobic effect,^[4] is sometimes observed. This phenomenon is explained in the viewpoint of the number of hydrogen bonds of water molecules. A solute molecule, especially large one, should decrease the number of hydrogen bonds because a hydrogen bond network avoiding the molecule is unlikely. This decrease will be proportional to the number of water molecules on the

surface of the solute molecule, whose formation of hydrogen bond is hindered. The number of such water molecules will be proportional to the surface area of the solute molecule. Aggregation of solute molecules decreases the number of such water molecules, increases the number of hydrogen bonds, and stabilizes the whole system enthalpically. This is a scenario of the enthalpy-driven hydrophobic effect.

Another factor causing the non-classical hydrophobic effect is the contribution of indirect van der Waals force, that is, van der Waals force that involves water molecules. As already stated, van der Waals force is a result of polarization induced by other molecules. Accordingly, we can understand that the intensity of van der Waals force is proportional to the product of the polarizabilities of two molecules. To maximize the total gain of van der Waals force, molecules with a large polarizability should interact with each other. When we compare the polarizability, that of water molecule is relatively smaller than that of carbon atom, a typical constituent of hydrophobic moieties. Therefore, if the difference of interatomic distance is negligible, aggregation of hydrophobic molecules should increase the total enthalpic gain by van der Waals force. This scenario is another possible explanation of the enthalpy-driven hydrophobic effect.

1.4. Construction of supramolecular structures by van der Waals force and the hydrophobic effect

1.4.1. Difficulties and meanings of supramolecular assembly by van der Waals interaction and the hydrophobic effect

Molecular recognition and non-covalent bond, including intermolecular interactions, are employed not only to natural systems but also to artificially constructed supramolecular structures. Hydrogen bond has been very often adopted in designs of supramolecular structures. ^[5] Many examples of supramolecular metal complexes are also reported, where organic ligands and metal ions are bonded by coordination bonds. ^[6] These intermolecular interactions are easy to employ because they are relatively strong, selective, and anisotropic. In other words, these interactions provide relatively strong attractive forces between desired moieties of components in a desired direction. This situation is required to construct a well-defined and unique supramolecular structure.

On the other hand, weak intermolecular interactions are less often employed because they are

weak, non-selective, and isotropic intermolecular interactions. Weak interactions cannot bind components effectively, resulting in a low affinity constant. Non-selective interaction can attract any pair of moieties, disabling to control the binding of components. Isotropic interactions allow components to aggregate in many configurations, complicating supramolecular design where components should gather in a specific configuration. These characters have prevented supramolecular scientists from utilizing these interactions to construct a well-defined and unique structure. This difficulty can be seen in the case of micelle and vesicle, typical examples of structures constructed by weak intermolecular interactions. In the formation of these structures, their size can be roughly controlled by designing the sizes of the hydrophobic part and the hydrophilic part of the amphiphilic monomer. Despite that, the strict control of the number of components of these structures has not been achieved.

Nevertheless, biological systems often manipulate these weak intermolecular interactions in their functions. With these interactions, they can recognize similar biomolecules that have almost the same ability to form hydrogen bond. For example, in a process of synthesis of protein, valine and isoleucine, which have only a small difference of one CH_2 group, are discriminated. Although the selectivity is contributed also by size effect and proofreading system, this molecular recognition should be enabled, at least partially, by means of the weak intermolecular interactions.

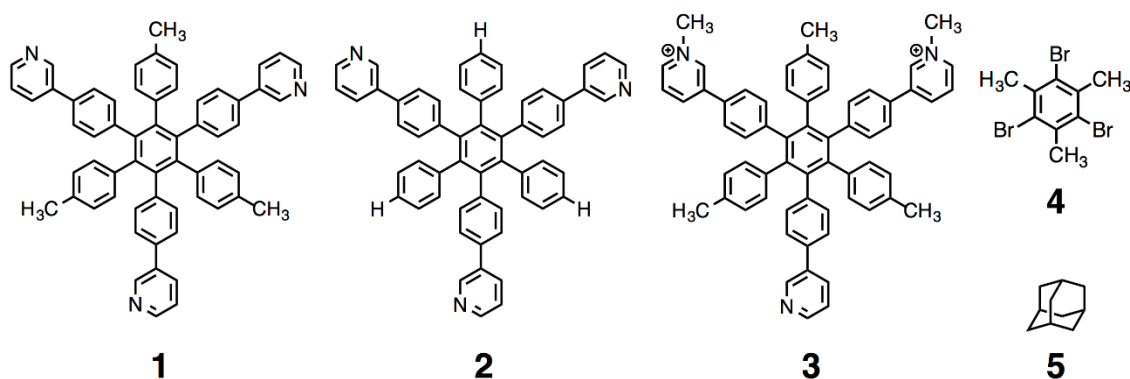
If a methodology to employ these interactions to construct supramolecular structure is established, the number of possible artificial supramolecular structures will drastically increase. Furthermore, more sophisticated system, as biological systems, will become achievable.

Today, only a few examples exist where such weak, non-selective, and isotropic interactions are sophisticatedly employed to obtain a well-defined and unique supramolecular structure. Gibb et al. reported the dimerization of a cavitand that possesses a hydrophilic external surface, a hydrophobic internal surface, and a hydrophobic rim.^[7] In the presence of a steroid molecule, this hemispheric molecule dimerizes into a capsule structure encapsulating the steroid molecule as a guest, dehydrating the internal surface, the rim, and the hydrophobic surface of the guest molecule. Sessler et al. reported the formation of an interlocked structure, [2]catenane, from two aromatic aldehyde molecules and two aromatic hydrazine molecules in aqueous media.^[8] Addition of organic solvent decomposed the structure and removal of organic solvent

regenerated the structure, indicating the importance of the hydrophobic effect. Hiraoka et al. reported another example, nanocube, which is introduced below.

1.4.2. Nanocube: an exceptional example

Nanocubes^[9 , 10 , 11] are supramolecular structures comprised of six molecules of hexaphenylbenzene derivatives. The first nanocube was discovered by dissolving **1** (Scheme 1-1) in aqueous methanol (water/methanol = 1/3 (v/v)). In this solution, six molecules of **1** hexamerize to a nanocube **1₆** (Figure 1-2(a)). The supramolecular structure of **1₆** in solution was confirmed by ¹H NMR, COSY, and DOSY. An ESI-TOF mass spectrum of methanolic solution of **1** showed the peaks of [**1₆** · Na_x]^{x+} (x = 2, 3, 4), suggesting the tendency of **1** to hexamerize. Single crystal X-ray diffraction (scXRD) technique revealed the detailed structure of nanocube **1₆**. Although a suitable crystal of **1₆** itself failed to be obtained, an inclusion complex with two molecules of tribromomesitylene **4** afforded a single crystal that can be analyzed by scXRD (Figure 1-2(a)). In the crystal structure, monomeric molecules **1** in **1₆** have broad molecular surface contacted to other monomer molecules, forming CH-π and π-π interactions. The CH-π interactions exist between the methyl groups and pyridine rings, whereas three pyridine rings of different monomer molecules stack and form π-π interactions. These contacts indicate the contributions of van der Waals force and the hydrophobic effect to the hexamerization.



Scheme 1-1. Hexaphenylbenzene derivatives, **1**, **2**, and **3**; guest molecules, tribromomesitylene **4** and adamantane **5**.

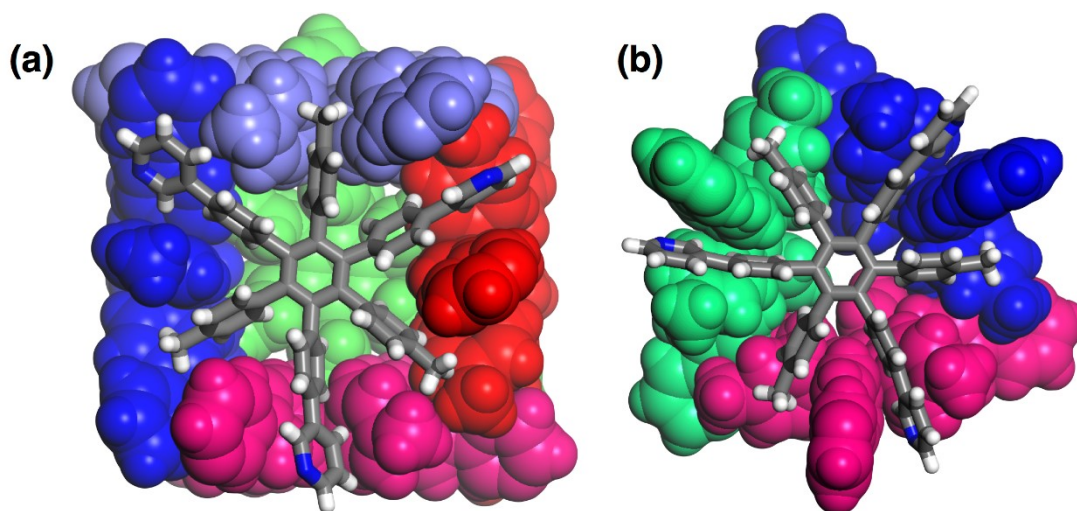


Figure 1-2. Crystal structures of (a) $1_6\supset 4_2$ and (b) $1_4\supset 5$. In each structure, one of the monomers is shown in stick model and the others in CPK model. For clarity, included guest molecules are omitted.

The driving force of this association behavior has been considered to be the hydrophobic effect (or more strictly, the solvophobic effect) and van der Waals force because **1** lacks moieties that cause any strong intermolecular interactions. The presence of water is essential because **1** exists as monomer in pure methanol. To investigate the driving force of the hexamerization more closely, the association constant of the nanocube **1**₆ was measured and the contributions of the enthalpy and the entropy to it were separately obtained by isothermal titration calorimetry (ITC) technique. Both of the enthalpy change ($\Delta H^\circ = -216 \text{ kJ mol}^{-1}$) and the entropy change ($\Delta S^\circ = -354 \text{ J mol}^{-1} \text{ K}^{-1}$) of the hexamerization of **1** were determined to be negative. This result showed that the hexamerization is enthalpy-driven. The driving force of the hexamerization of **1** is therefore the non-classical hydrophobic effect, including van der Waals force caused by the broad molecular surface contacted to other monomer molecules, rather than the classical hydrophobic effect, which is entropy-driven. The negative entropy change can be explained by the degree of freedom and the solvent. In the association process, 15 rotational degrees of freedom and 15 translational degrees of freedom are converted into 30 vibrational degrees of freedom that correspond to the change of the relative positions of the monomers. The vibrational degrees of freedom in the associated form are more constrained than the rotational and translational ones in the dissociated form because the associated monomers cannot travel apart from the other monomers. This effect is especially important in the nanocube system

because of the broad contacted surface. Additionally, the solvent is not pure water but a mixture of water and methanol, much weakening the hydrophobic effect that would have a large positive contribution to the entropy change.

Interestingly, the methyl groups of **1** are essential to the formation of the nanocube. A methyl group is relatively rather small compared with the hexaphenylbenzene core. However, **2**, a derivative of **1** that lacks the methyl groups, did not form any aggregate in aqueous methanol. This phenomenon offers an important insight: a relatively small part of components can be essential to an aggregation behavior.

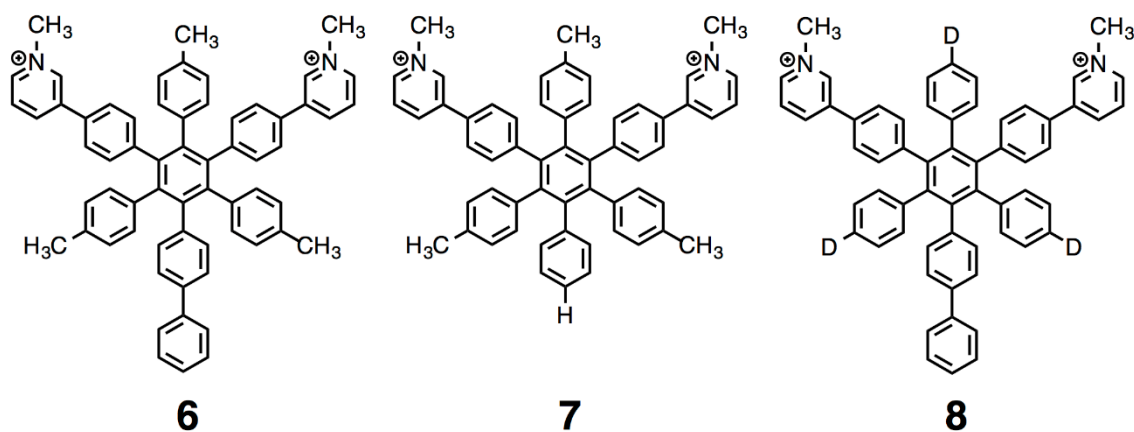
The association constant of **1** is strongly affected by the ratio of water in solvent because the hydrophobic effect drives the aggregation of **1**. On the addition of water into the methanolic solution of **1**, gradual aggregation of **1** was observed. However, the ratio of water was limited by the solubility of **1** because **1** is not sufficiently hydrophilic and cannot be dissolved in water. If **1** were more soluble in pure water, much more high value of association constant would be observed with the enhanced hydrophobic effect.

To overcome this limitation, a more hydrophilic derivative **3** was developed. The monomer **3** has two *N*-methylpyridinium moieties and a neutral pyridine ring, instead of the three pyridine rings of **1**. By the methylation from **1** to **3**, the amphiphilic molecule becomes ionic, more hydrophilic, and soluble in pure water. As expected, the amphiphile **3** exists as monomer in pure methanol and as nanocube **3**₆ in pure water. The nanocube **3**₆ is so stable that dilution to 1 μM cannot dissociate it, preventing the determination of the association constant of **3**₆ by ITC. This higher stability of **3**₆ than **1**₆ will be contributed by two factors. The abovementioned enhanced hydrophobic effect in pure water realized in the case of **3**₆. Three aromatic rings stacked as pyridinium-pyridine-pyridinium in **3**₆, instead of pyridine-pyridine-pyridine in **1**₆, form not only π - π interaction but also cation- π interaction, further stabilizing **3**₆.

Another example indicating the importance of contact surface is an altered association behavior of **1** in the presence of a guest. When adamantane **5** coexists, tetrahedral tetramer **1**₄ (Figure 1-2(b)) was observed instead of the hexamer. The reason of the altered association behavior is considered to be the maximization of van der Waals force, that is, the maximization of contact surface area. The tetramer seems to possess smaller contact surface area than the hexamer, because the π - π stack motifs are lost in the tetramer. However, the decrease of the

contact surface area between the host structure can be compensated or even overcome by the contact between the host and the guest molecule. In this case, the similar tetrahedral structures of the tetramer and adamantane enable large part of the interior surface of the host and the surface of the guest to become contact surface. This larger host-guest contact makes the formation of the tetramer complexed with adamantane more favored than the formation of the hexamer.

Recently, other types of nanocubes, **6**₆, **7**₆, and **8**₆, were developed (Scheme 1-2).^[12] The monomer **6** and **7** have a benzene ring and a hydrogen atom, respectively, instead of the pyridine ring of **3**. The monomer **8** has three deuterium atoms, instead of three methyl groups of **6**. These three monomers hexamerize into nanocubes in pure water. The stabilities of these nanocubes, along with **3**₆, were investigated (Table 1-1). The disassembly temperatures (T_d), the temperatures at which half of the amphiphilic molecules exist as monomer, were determined by NMR. The Gibbs energy changes of the association reactions at 298 K (ΔG_a^0) were determined by ITC. These stability parameters show that **3**₆ and **6**₆ are more stable than **7**₆ and **8**₆, indicating that three methyl groups and three aromatic rings are important to the high stability of a nanocube. These structures will contribute to van der Waals force and stabilize the nanocube structure, such as **3**₆ and **6**₆. The higher stability of **6**₆ than **3**₆ can be explained by stronger cation- π interaction between a benzene ring and pyridinium rings in **6**₆ than that between a pyridine, less negative than benzene, and pyridinium rings in **3**₆. All of these interactions, van der Waals force and electrostatic interaction, as well as the hydrophobic effect, effectively work in the formation of the very stable supramolecular structure, nanocube **6**₆.



Scheme 1-2. Recently synthesized hexaphenylbenzene derivatives, **6**, **7**, and **8**, which form nanocube in water.

Table 1-1. Thermal stabilities of water-soluble nanocubes.

Nanocube	T_d / K	ΔG_a^0 / kJ mol ⁻¹
3 ₆	385	—[a]
6 ₆	403	—[a]
7 ₆	313	-111.8
8 ₆	338	-142.1

[a] unable to determine because of high stability

The specialty of the nanocubes, among the supramolecular structures utilizing weak intermolecular interactions, is the uniqueness of the obtained structure, that is, only hexamer is obtained and the others such as pentamer or dodecamer are not obtained. Weak intermolecular interactions usually do not show such uniqueness, as can be seen in the case of micelle or vesicle. The uniqueness of the structure of the nanocubes should arise from the shape of the monomers, **1** and **3**. The shape requires limited configuration of the monomers to achieve effective van der Waals force and offers the large area of the contact surface. These facts overcome the difficulties of utilization of weak intermolecular interactions, their isotropic nature and weakness.

1.5. Prediction of affinity

1.5.1. Importance of contact surface areas

To deeply understand molecular recognition and apply it to various fields, the evaluation of the association affinity of a given system is important. This is because molecular recognition is a phenomenon resulting from sufficient differences of association affinities of several guests to the host. Precise and quantitative evaluation and prediction of association constants can be regarded as a key to understanding and application of molecular recognition. The association constant is determined by the intensity of intermolecular interactions. The weak intermolecular interactions become especially important because they are universal, that is, always exist regardless of the kind of component atoms. The energetic contribution of these interactions is considered to have proportional correlation with the area of contact surface of the system. This correlation has been widely investigated and confirmed.^[3,13]

Houk et al.^[14] have maintained the existence of a universal linearity that holds in various host-guest systems. They gathered many reports on the association constants of host-guest systems and calculated the contact surface areas of these systems. These sets of values of the association constant and contact surface area were classified according to the category of the system, such as cyclodextrin systems, protein-substrate systems, and so on. In each category, the association constants and contact surface areas were averaged. This process derived the sets of the averaged association constants and the averaged contact surface areas of each category. When these averaged association constants were plotted against contact surface areas, a linear correlation appeared (Figure 1-3).

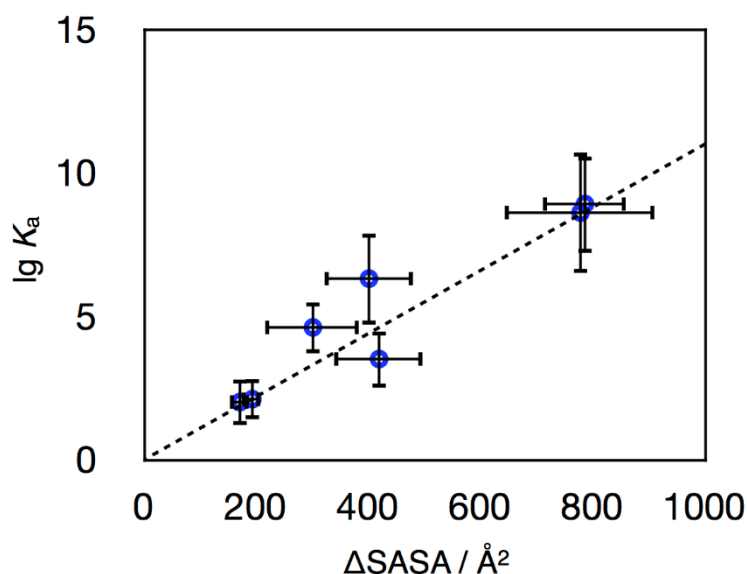


Figure 1-3. Plot of the averaged association constants against contact surface area.^[14] The dashed line is the trend line of the plotted data. The error bars indicate standard deviations.

1.5.2. Importance of intersurface distance

Not only contact surface area, as stated in the previous section, but also other factors should significantly affect the association constant. Houk et al. have shown the universal linear correlation between the contact surface area and the association constant. However, some observed values of association constants described in their report considerably deviate from the predicted ones from the linear correlation. This deviation indicates that contact surface area alone is insufficient to precisely predict the association constant of a given molecular system.

One of the probable factors affecting association constant is intersurface distance. This effect should exist because intersurface distance strongly alters the intensity of van der Waals force, which is ubiquitous and should always be considered. An optimum intersurface distance maximizes the intensity of van der Waals force. A deviation from this optimum value will largely decrease this stabilization by van der Waals force. To understand this mechanism more visually, consider two binary complexes in water, shown in Figure 1-4. Both of the complexes have similar contact surface areas. The degree of the classic hydrophobic effect should therefore be similar. Nevertheless, the intensity of the van der Waals force between the components of the complex can be different. In (a), the intersurface distance is small and the binding is tight,

whereas the opposite is true in (b). This difference of van der Waals force will stabilize more (a) than (b). The total association affinity of (a) will therefore be larger than that of (b).

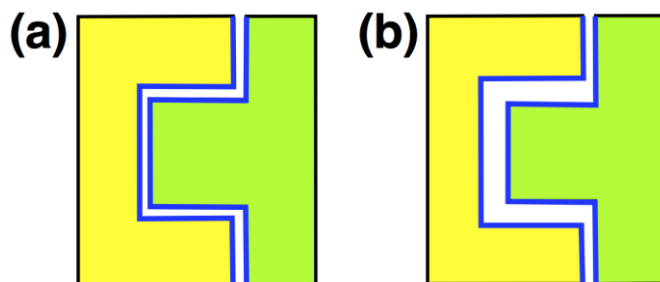


Figure 1-4. Two schematic examples of binary complexes with similar contact surface areas (indicated by the blue lines) and different intersurface distances.

Consideration of the intersurface distance should be indispensable for precise prediction of the association constant. In my best knowledge, however, a method with such consideration has not been proposed. A novel method to evaluate and visualize the distribution of intersurface distance of a given structure can refine and facilitate the prediction of the association constant.

1.6. Aim of the thesis

In the previous sections, the importance of quantitative estimation of association affinity is explained. Literature studies on the topics and their limitations are also introduced.

This thesis describes the development of a novel method, Surface Analysis with Various Probe Radius, SAVPR. This method can semiquantitatively evaluate and visualize the tightness of the contact surface of a given structure.

In Chapter 2, the concept and formulation of SAVPR are explained. To investigate contact surface areas, types of molecular surface should be specified. This chapter introduces three types of molecular surface. A formula to obtain intersurface distance distribution is also given.

In Chapter 3, SAVPR is applied to rationalization of the deviation from a trend that describes the proportional relationship between association constants and contact surface areas of host-guest systems. This deviation can be explained by the tightness of the contact surface, which can be evaluated by SAVPR.

In Chapter 4, SAVPR is applied to a novel nanocube and the effect of a small structural

difference on the association affinity is investigated. Small difference can affect the tightness of the contact surface and hence association affinity.

In Chapter 5, the series of these studies are summarized and the future prospects are mentioned.

References and Notes

- ¹ a) Wöhler, F. *Poggendorffs Ann.* **1828**, *12*, 253–256; b) Cohen, P. S.; Cohen, S. M. *J. Chem. Educ.* **1996**, *73*, 883–886.
- ² London, F. *Trans. Faraday Soc.* **1937**, *33*, 8–26.
- ³ Southall, N. T.; Dill, K. A. *J. Phys. Chem. B.* **2000**, *104*, 1326–1331.
- ⁴ Meyer, E. A.; Castellano, R. K.; Diederich, F. *Angew. Chem., Int. Ed.* **2003**, *42*, 1210–1250.
- ⁵ a) Desiraju, G. R. *Acc. Chem. Res.* **1996**, *29*, 441–449; b) Conn, M. M.; Rebek, J. Jr. *Chem. Rev.* **1997**, *97*, 1647–1668; c) Brunsveld, L.; Folmer, B. J. B.; Meijer, E. W.; Sijbesma, R. P. *Chem. Rev.* **2001**, *101*, 4071–4098; d) Sherrington, D. C.; Taskinen, K. A. *Chem. Soc. Rev.* **2001**, *30*, 83–93; e) Armstrong, G.; Buggy, M. *J. Mater. Sci.* **2005**, *40*, 547–559.
- ⁶ a) *Templating, self-assembly, and self-organization*; Sauvage, J.-P.; Hosseini, M. W., Eds.; Comprehensive Supramolecular Chemistry, Vol. 9; Elsevier: Oxford, 1996. (Especially, Chapter 2, 5, 6, and 7); b) Caulder, D. L.; Raymond, K. N. *J. Chem. Soc., Dalton Trans.* **1999**, 1185–1200; c) Leininger, S.; Olenyuk, B.; Stang, P. J. *Chem. Rev.* **2000**, *100*, 853–908; d) Ward, M. D. *Annu. Rep. Prog. Chem., Sect. A: Inorg. Chem.* **2000**, *96*, 345–385; e) Fujita, M.; Tominaga, M.; Hori, A.; Therrien, B. *Acc. Chem. Res.* **2005**, *38*, 369–378; f) Saalfrank, R. W.; Maid, H.; Scheurer, A. *Angew. Chem., Int. Ed.* **2008**, *47*, 8794–8824; g) S. J. Dalgarno, N. P. Power, J. L. Atwood, *Coord. Chem. Rev.* **2008**, *252*, 825–841; h) R. Chakrabarty, P. S. Mukherjee, Stang, P. J. *Chem. Rev.* **2011**, *111*, 6810–6918; i) H. Amouri, C. Desmarets, J. Moussa, *Chem. Rev.* **2012**, *112*, 2015–2041; j) T. R. Cook, Y.-R. Zheng, P. J. Stang, *Chem. Rev.* **2013**, *113*, 734–777; k) M. M. J. Smulders, I. A. Riddell, C. Browne, J. R. Nitschke, *Chem. Soc. Rev.* **2013**, *42*, 1728–1754; l) T. R. Cook, P. J. Stang, *Chem. Rev.* **2015**, *115*, 7001–7045. m) W. Wang, Y.-X. Wang, H.-B. Yang, *Chem. Soc. Rev.* **2016**, *45*, 2656–2693.
- ⁷ Gibb, C. L. D.; Gibb, B. C. *J. Am. Chem. Soc.* **2004**, *126*, 11408–11409.
- ⁸ Li, H.; Zhang, H.; Lammer, A. D.; Wang, M.; Li, X.; Lynch, V. M.; Sessler, J. L. *Nat. Chem.* **2015**, *7*, 1003–1008.
- ⁹ Hiraoka, S.; Harano, K.; Shiro, M.; Shionoya, M. *J. Am. Chem. Soc.* **2008**, *130*, 14368–14369.
- ¹⁰ Hiraoka, S.; Harano, K.; Nakamura, T.; Shiro, M.; Shionoya, M. *Angew. Chem., Int. Ed.* **2009**, *48*, 7006–7009.
- ¹¹ Hiraoka, S.; Nakamura, T.; Shiro, M.; Shionoya, M. *J. Am. Chem. Soc.* **2010**, *132*, 13223–13225.
- ¹² Zhan, Y.-Y.; Ogata, K.; Kojima, T.; Koide, T.; Mashiko, T.; Tachikawa, M.; Hiraoka, S. submitted.
- ¹³ a) Cohen, J. L.; Connors, K. A. *J. Pharm. Sci.* **1970**, *59*, 1271–1276; b) Hermann, R. B. *J. Phys. Chem.* **1972**, *76*, 2754–2759; c) Harris, M. J.; Higuchi, T.; Rytting, J. H. *J. Phys. Chem.* **1973**, *77*, 2694–2703; d) Reynolds, J. A.; Gilbert, D. B.; Tanford, C. *Proc. Natl. Acad. Sci.* **1974**, *71*, 2925–2927; e) Yaacobi, M.; Ben-Naim, A. *J. Phys. Chem.* **1974**, *78*, 175–178; f) Abraham, M. H. *J. Am. Chem. Soc.* **1982**, *104*, 2085–2094; g) Sharp, K. A.; Nicholls, A.; Fine, R. F.; Honig, B. *Science* **1991**, *252*, 106–109; h) Sharp, K. A.; Nicholls, A.; Friedman, R.; Honig, B. *Biochemistry* **1991**, *30*, 9686–9697; i) Searle, M. S.; Williams, D. H.; Gerhard, U. *J. Am. Chem. Soc.* **1992**, *114*, 10697–10704; j) Böhm, H.-J. *J. Comput.-Aided Mol. Design* **1994**, *8*, 243–256; k) Novotny, J.;

Brucoleri, R. E.; Davis, M.; Sharp, K. A. *J. Mol. Biol.* **1997**, *268*, 401–411; l) Raschke, T. M.; Tsai, J.; Levitt, M. *Proc. Natl. Acad. Sci.* **2001**, *98*, 5965–5969; m) Kyte, J. *Biophysical Chemistry* **2003**, *100*, 193–203; Whitehead, M.; Turega, S.; Stephenson, A.; Hunter, C. A.; Ward, M. D. *Chem. Sci.* **2013**, *4*, 2744–2751.

¹⁴ Houk, K. N.; Leach, A. G.; Kim, S. P.; Zhang, X. *Angew. Chem., Int. Ed.* **2003**, *42*, 4872–4897.

Chapter 2.

Development of Surface Analysis with Various Probe Radius (SAVPR) Method

This chapter deals with evaluation of contact surface area, which strongly affect the intermolecular interactions and molecular recognition. This chapter introduces Surface Analysis with Various Probe Radius (SAVPR) method, a novel method to evaluate the contact surface area of a given structure

The evaluation of contact surface area requires the concept of molecular surface area. Three kinds of molecular surface area have been proposed.^[1] In the first section, these three molecular surfaces are introduced. The next section introduces the novel method, SAVPR, on the basis of the concept of molecular surface.

2.1. Three types of molecular surface

There are several concepts to represent molecular surface. Although they represent a similar shape for the same molecule, they have some difference. Here, three types of molecular surface are introduced: van der Waals (vdW) surface, Connolly surface, and solvent accessible surface.

2.1.1. van der Waals surface

Among the three types of molecular surface, vdW surface is the most fundamental and widely adopted. In this concept, atoms are viewed as a sphere and molecules are simply viewed as overlapped spheres that represent atoms (Figure 2-1(a)). The radii of the spheres are decided according to the type of the atoms, such as the kind of elements and their chemical environments. These radii are referred to as vdW radii.

2.1.2. Connolly surface

Connolly surface^[2] is defined based on vdW surface. To obtain Connolly surface, a probe sphere, which cannot overlap with the atoms of their vdW radii in a given structure, is rolled over the structure. Connolly surface is thus obtained as the boundary surface of the domain into which a probe sphere cannot enter (Figure 2-1(b)).

Connolly surface and vdW surface have a similarity and a difference. The convex parts of Connolly surface coincide with those of vdW surface. On the other hand, contacted vdW surface of a smaller intersurface distance than the probe diameter cannot be touched by the probe sphere, and hence excluded from Connolly surface. This fact means Connolly surface area can be affected the relationship between the probe diameter and the intersurface distance.

As noted later, Connolly surface is employed in the SAVPR method.

2.1.3. Solvent accessible surface

Solvent accessible surface^[3] (also referred to as Lee-Richards accessible surface) is defined similarly to Connolly surface: while a probe sphere is used in the same manner as Connolly surface, solvent accessible surface is defined as the locus of the center of the probe sphere, which is an approximation of solvent molecules (Figure 2-1(c)). While the shapes of these two surfaces are similar, solvent accessible surface is usually larger as seen in the figure.

Solvent accessible surface have been commonly employed in evaluation of contact surface area. This is because solvent accessible surface corresponds to the curvature constituted from solvent molecules solvating the target molecule. This correspondence means that solvent accessible area should be proportional to the number of solvent molecules that directly solvates the target molecule, which should be also proportional to the free energy change by solvent effect such as the hydrophobic effect.

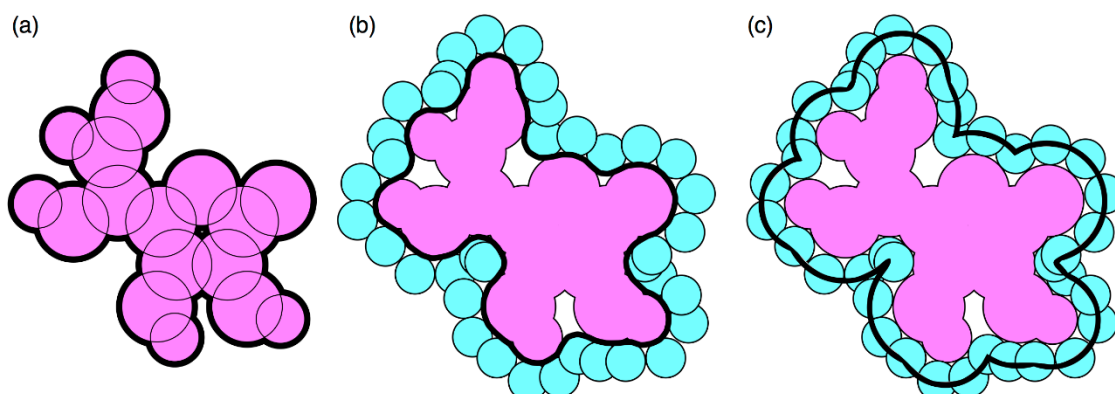


Figure 2-1. Three types of molecular surface: (a) vdW surface, (b) Connolly surface, (c) solvent accessible surface. Black thick lines represent the corresponding molecular surfaces.

2.2. Surface Analysis with Various Probe Radius (SAVPR) method

2.2.1. Concept

In this thesis, the author proposes an efficient method to calculate and visualize the intersurface distance distribution of a given structure, Surface Analysis with Various Probe Radius (SAVPR). With Connolly surface areas, this method classifies contact surface into tightly or loosely contacted surface. This difference of tightness of contact surface will explain the different strength of intermolecular interaction, especially vdW interaction.

To evaluate the intersurface distance distribution by means of the SAVPR method, the Connolly surface areas with various probe radii of an associated form and a dissociated form are calculated and the difference of these two values is obtained. This difference is a function of the probe radius and this function means the contact surface areas whose intersurface distance is less than the probe diameter. By differentiating this function, the intersurface distance distribution can be obtained.

The characteristic point of this method is usage of various sizes of probe sphere. In the previous studies, more than one probe radius have been seldom employed. One of a few examples have been reported by Dowejko and Johnson.^[4] In order to quantify the hydrophobic effect, they proposed a method to quantify the degree of freedom of solvent molecules. They compared the results derived from their method with ones from calculation of contact surface areas. In their calculation of solvent accessible surface areas, they employ two radii, a typical value of 1.4 Å and a smaller value of 0.5 Å. The smaller radius of 0.5 Å gave similar result with their method and succeeded in predicting the most close structure to crystal structure among the candidate structures calculated from different initial configurations of the complex in question, whereas established value of 1.4 Å failed. This research encouraged the usage of smaller probe radius in SAVPR.

In the next subsection, the detailed formulation of the SAVPR method is given. Its application to real systems and proof of the usefulness are shown in the following chapters.

2.2.2. Formulation

As mentioned above, the derivation of the distribution of intersurface distance by means of SAVPR is based on the calculation of Connolly surface area. First, $A_{as}(D)$ and $A_{dis}(D)$ are

defined as the Connolly surface area of the associated form and the dissociated form, respectively, of a given structure with a probe sphere of diameter D (Figure 2-2). Then, $A(D)$ is defined as the difference of these two values:

$$A(D) := A_{\text{dis}}(D) - A_{\text{as}}(D)$$

A probe sphere of diameter D cannot enter the intersurface space whose intersurface distance is less than D . In other words, a part of contact surface whose intersurface distance is less than D is excluded from the Connolly surface area of the associated form obtained with a probe sphere of diameter D . From this consideration, $A(D)$ can be viewed as the contact surface whose intersurface distance is less than D . Therefore, the area of the contact surface of the intersurface distance between D and $D + \Delta D$ can be estimated to $A(D + \Delta D) - A(D)$:

$$\text{ContactSurfaceArea}(D, D + \Delta D) = A(D + \Delta D) - A(D)$$

where ΔD is the interval of intersurface distance. From this relation, the histogram of intersurface distance, intersurface distance distribution, can be drawn.

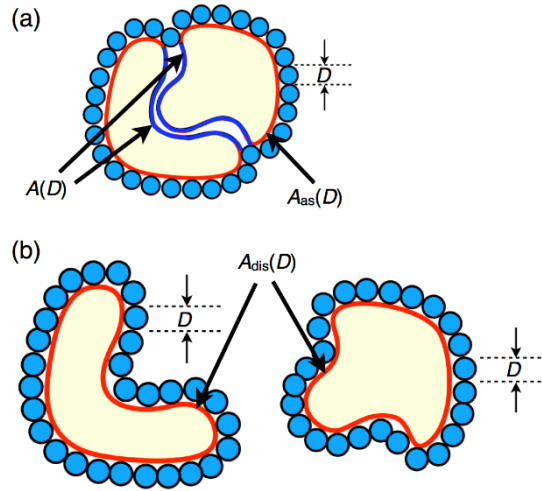


Figure 2-2. Schematic representation of the SAVPR method. (a) associated form of a given structure; (b) dissociated form of the structure. Light blue circles are probe spheres. The part of the surface shown as red line is the Connolly surface of this structure, while the one shown as blue line is the contact surface whose intersurface distance is less than D . $A_{\text{as}}(D)$ is defined as the area of the Connolly surface area of the associated structure and $A_{\text{dis}}(D)$ is defined as the total Connolly surface area of the dissociated structure. $A(D)$ is defined as the difference of $A_{\text{as}}(D)$ and $A_{\text{dis}}(D)$, which is (almost)^[5] equal to the contact surface.

In the ideal sense, $A'(D)$ is the intersurface distance distribution. For any sufficiently small ΔD ,

$$\text{ContactSurfaceArea}(D, D + \Delta D) = A(D + \Delta D) - A(D) \sim A'(D) \Delta D$$

While $A(D + \Delta D) - A(D)$ is dependent on ΔD , $A'(D)$ is not. This independency shows that adopting $A'(D)$ as intersurface distance distribution excludes the arbitrary of the choice of ΔD . In practical calculation, infinitesimal ΔD cannot be chosen and the arbitrary should remain. To minimize that, adequate approximation of $A'(D)$ is given. First, σ is defined as follows:

$$\sigma(D) := A\left(D + \frac{\Delta D}{2}\right) - A\left(D - \frac{\Delta D}{2}\right),$$

or

$$\sigma\left(D + \frac{\Delta D}{2}\right) := A(D + \Delta D) - A(D).$$

By expanding the right hand,

$$\begin{aligned} \sigma(D) &= A\left(D + \frac{\Delta D}{2}\right) - A\left(D - \frac{\Delta D}{2}\right) \\ &= \left(A(D) + \frac{\Delta D}{2} A'(D) + \frac{1}{2} \left(\frac{\Delta D}{2}\right)^2 A''(D) \right) - \left(A(D) - \frac{\Delta D}{2} A'(D) + \frac{1}{2} \left(\frac{\Delta D}{2}\right)^2 A''(D) \right) \\ &\quad + O((\Delta D)^3) \\ &= A'(D) \Delta D + O((\Delta D)^3) \end{aligned}$$

Therefore,

$$\frac{\sigma(D)}{\Delta D} = A'(D) + O((\Delta D)^2)$$

This expression shows that $\sigma(D)/\Delta D$ can approximate $A'(D)$ for sufficiently small ΔD . This function $A'(D)$ is essentially independent of ΔD , aside from the interval of data. This independency indicates that, when $\sigma(D)/\Delta D$ is regarded as the intersurface distance distribution, its intensity hardly depends on ΔD anymore.

As a simpler definition, the term of ΔD can be omitted, that is, $\sigma(D)/\Delta D$ can be regarded as the intersurface distance distribution.

$$\text{ContactSurfaceArea}(D, D + \Delta D) = A(D + \Delta D) - A(D) = \sigma(D + \Delta D/2)$$

When this definition of intersurface distance distribution is adopted, the intensity of the distribution depends on ΔD . As noted later, the value of ΔD should be determined according to the system. The dependency on ΔD and different value of ΔD can be problematic because direct

comparison of intersurface distance distributions of many systems may become impossible. However, if target structures possess a similar size, a common ΔD value can be applied and $\sigma(D)$, not $\sigma(D)/\Delta D$, can be directly compared. Adopting this simpler definition facilitates and simplifies the calculation process. This simplified process is adopted in the actual calculation of this study.

The interval of the diameter of the probe sphere, ΔD , should be selected according to calculation environment and a system in question. Smaller ΔD gives more detailed structures of intersurface distance distributions. However, it decreases the value of $A(D + \Delta D) - A(D)$, making the calculation result vulnerable to the error of the areas. When ΔD becomes smaller than the accuracy of the calculated area, the resulting distribution of contact surface will be largely affected by numerical errors. Also, too small ΔD also causes the increase of calculation time, spoiling the efficiency of SAVPR, especially in larger systems requiring long calculation time. This requirement practically prevents us from selecting as small ΔD value in large system as we can in smaller systems. These considerations show that ΔD should be moderately small and sufficiently larger than the fluctuation of the calculated area. The restriction of ΔD encourages us to adopt different ΔD values according to the size of systems. In this thesis, common value of $\Delta D = 0.02 \text{ \AA}$ is adopted because all of the systems have similar sizes. In this study, $A(D)$ is calculated by every 0.02 \AA from $D = 0 \text{ \AA}$ to $D = 3.00 \text{ \AA}$. From this data, we calculated $\sigma(D)$ from $D = 0.01 \text{ \AA}$ to $D = 2.99 \text{ \AA}$. With $\sigma(D)$, we can discuss the contact surface, taking the intersurface distance into consideration.

2.2.3. Features

The SAVPR is a novel method to evaluate the affinity of a given associated structure in that the method considers not only the contact surface area but also further detail of a given structure. This feature will contribute to the improvement of the prediction of the association affinity.

The SAVPR method can be applied via simple steps. All the essential calculation of the SAVPR method is the evaluation of the Connolly surface areas of the given structures with various probe radii. This evaluation can be achieved only by inputting the given structure into software available today. By simply differentiating the Connolly surface areas with the probe diameter D , the intersurface distance distribution can be obtained. As a result, the relation

between the detail of the structure and the distribution is implicit, i.e., the domain of intersurface distance that a certain part of the structure mainly affects in the distribution is not directly shown. This point can be a drawback when such relationship should be discussed. Nevertheless, this point can be also an advantage because, once the users of the SAVPR method obtain the intersurface distance distribution, they do not need to explicitly discuss the detail of the structure when they only need the distribution.

In the following two chapters, examples of application of the SAVPR method are shown and the utility of the SAVPR method is demonstrated.

References and Notes

¹ Kim, D.-S.; Won, C.-I.; Bhak, J. *J. Biomol. Struct. Dyn.* **2010**, *28*, 277–287.

² Connolly, M. L. *Science* **1983**, *221*, 709–713.

³ Lee, B.; Richards, F. M. *J. Mol. Biol.* **1971**, *55*, 379–400.

⁴ Doweyko, A. M.; Johnson, S. R. *J. Chem. Inf. Model.* **2006**, *46*, 2563–2573.

⁵ $A(D)$ is not strictly equal to contact surface area because Connolly surfaces include not only the vdW surface of the molecules but also some other parts which are off the concave parts of the vdW surface.

Chapter 3.

Effect of Intersurface Distance Density on Association Affinity

(This chapter is partially reproduced from Ref. 1 with permission from the Royal Society of Chemistry.)

The previous chapter has introduced SAVPR, the novel method to evaluate the contact surface area of a given structure. In that chapter, the concept of SAVPR is explained and the formulation is given.

In this chapter, some supramolecular systems are analyzed by the SAVPR method and its applicability is confirmed.

3.1. Introduction

Intermolecular interactions play an essential role in various phenomena such as molecular recognition. Aside from molecular recognition noted in Section 1.2, formation of micelle and vesicle,^[2] protein folding,^[3] and enzyme-substrate system^[4] are driven by weak intermolecular interactions. Although only a few examples exist as mentioned in Section 1.4, these interactions play an important role in several artificial systems for self-assembly^[5] and selective recognition of small molecules.^[6] Profound understanding of the natural systems and facilitation of the design of supramolecular structures should be provided by the development of a method with which the strength of these interactions in a given structure can be easily estimated. Such a method can be applied to wide disciplines and industrial field, for example, to the development of novel drugs.

In the estimation of weak intermolecular interactions, simple comparisons of contact surface area based on solvent accessible surface have been conducted. Especially, the Gibbs energy change by the hydrophobic effect has been assumed to be proportional to the contact surface area of the given system, as noted in Section 1.3. In this context, contact surface area is evaluated as the change of solvent accessible surface area (SASA) between before and after association. Hereafter, this change of SASA is written as Δ SASA and regarded as contact surface area. Houk et al.^[7] surveyed contact surface areas between before and after association, and association energies of many host-guest complexes. They found a proportional relation between these two

parameters as follows:

$$\text{Gibbs Energy Change} \propto \log_{10} K_a = 0.011 \times (\text{contact surface area} / \text{\AA}^2)$$

However, adequately precise evaluation of the strength of weak intermolecular interactions must require not only contact surface area, which is the only information used in the abovementioned method, but also some other information about the contact surface. In fact, Mizutani et al.^[8] pointed out that the reported values of Gibbs energy change per surface area in association process vary in a very wide range (0.084 – 0.38 kJ·mol⁻¹·Å⁻²). This great variation suggests the contribution of the detailed structure of the contact surface such as intersurface distance, which should strongly affect the vdW force, to the association energy.

In this chapter, the influence of intersurface distance on weak intermolecular interactions is proven by the SAVPR method. First, an example of nanocubes where simple comparison of contact surface area fails to predict the strengths of association affinities is introduced. This failure is explained by intersurface distance distributions of nanocubes. To show that short intersurface distance may greatly strengthen the association affinity, the SAVPR method is applied to some host-guest systems, as well as nanocubes. These considerations emphasize the importance of intersurface distance and the applicability of the SAVPR method.

3.2. Analysis of contact surface areas of nanocubes

The importance of the detailed structure of the contact surface in hydrophobically assembling systems was implied in the formation of a nanocube. As noted in Section 1.4, the amphiphile **1** spontaneously and hydrophobically assembles into a nanocube **1₆** in aqueous methanol, while its analog **2**, only without three methyl groups, does not. Because the presence of the three methyl groups should result in only a little difference in the contact surface areas of **1₆** and **2₆**, the different assembling behavior of **1** and **2** cannot be explained only by the difference in the contact surface areas.

This fact was successfully proven numerically by comparing the contact surface areas of **1₆** and **2₆** with the strength of experimentally determined association constants (Table 3-1). The ratio of the contact surface area of **1₆** to that of **2₆** is about 1.16:1. The association constant, K_a of **1₆** was previously determined by isothermal titration calorimetry (ITC) as $K_a(\mathbf{1}_6) = 3.2 \times 10^{19} \text{ M}^{-5}$ or $\log_{10} K_a(\mathbf{1}_6) = 19.5$. Contrary to **1**, the exact value of association constant of **2** cannot be

obtained experimentally because the 2.0 mM solution of amphiphile **2** did not exhibit any sign of the association on ^1H NMR measurement. Considering the sensitivity of NMR measurement, it was assumed that at most only 5% of amphiphile **2** assembled into the nanocube in the solution. This assumption allowed the deduction that $K_a(\mathbf{2_6}) < 3.54 \times 10^{11} \text{ M}^{-5}$ or $\log_{10} K_a(\mathbf{2_6}) < 11.5$ (the detail of the calculation is shown in Section 3.5). Accordingly, the association Gibbs energy, which is proportional to $\log_{10} K_a$, of **1₆** is at least 1.68-fold greater than that of **2₆**. This ratio is quite larger than that of the contact surface areas of **1₆** and **2₆**. In other words, if association Gibbs energy changes were proportional to contact surface areas, **2** would associate in more than 5%. This assumption obviously contradicts with the observed absence of aggregate of **2**. This discrepancy strongly supports the hypothesis that contact surface area is not the exclusive factor that determines the strength of the solvophobic effect and demands the consideration of the detailed structure of contact surface for the evaluation of associated structures.

The same discussion applies to the cationic nanocubes introduced in Section 1.4.2, for example, **6₆** and **8₆**. Although the actual value of the association constant of **6₆**, $K_a(\mathbf{6_6})$, was not obtained because of its high stability, its lower limit can be obtained as $K_a(\mathbf{6_6}) > 2.56 \times 10^{39} \text{ M}^{-5}$ or $\log_{10} K_a(\mathbf{6_6}) > 39.4$ (cf. Section 3.5). From this consideration, the association Gibbs energy of **6₆** should be at least 1.58-fold greater than that of **8₆**, whereas the contact surface area of **6₆** is only 1.17-fold greater than that of **8₆**.

Table 3-1. The contact surface areas and the common logarithms of association constants ($\log_{10} K_a$) of nanocubes.

Amphiphile	Contact surface area / \AA^2	$\log_{10} K_a$	Solvent
1	1960.9	19.5	Water/methanol ^[a]
2	1690.8	<11.5 ^[b]	Water/methanol ^[a]
3	2110.4	>39.4 ^[b]	Water
6	2129.3	>39.4 ^[b]	Water
7	1715.5	19.6	Water
8	1821.2	24.9	Water

[a] Water/methanol = 1/3 (v/v).

[b] These values are upper or lower limit (cf. Section 3.5).

3.3. Analysis of intersurface distance

3.3.1. Nanocubes in aqueous methanol

From the intersurface distance distributions of **1₆** and **2₆** obtained by means of SAVPR, the contact surface of **1₆** is proven not only larger but also tighter than that of **2₆**, i.e., **1₆** possesses much larger contact surface of short intersurface distance (<2 Å) than **2₆** (Figure 3-1). Such close contact surface should result in stronger vdW force than that of long intersurface distance (>2 Å). This strong interaction of **1₆** should be the origin of its larger association energy than that of **2₆** and can explain the discrepancy between the ratio of contact surface areas and that of association energies.

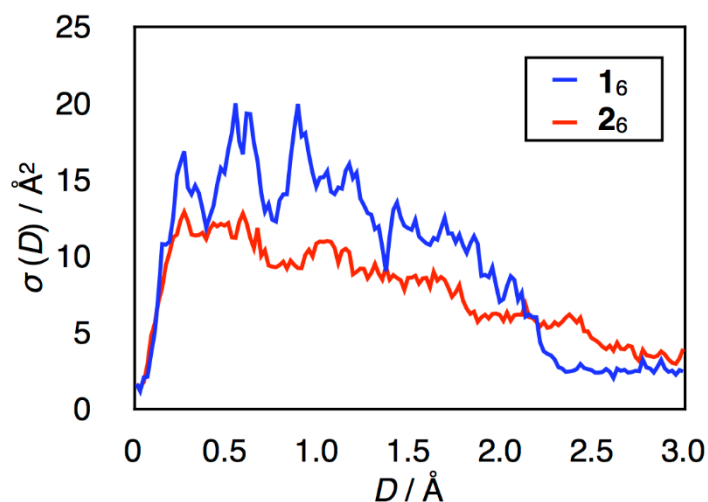


Figure 3-1. Intersurface distance distribution $\sigma(D)$ for **1₆** and **2₆**.

3.3.2. Nanocubes in pure water

The intersurface distance distributions of **3₆**, **6₆**, **7₆**, and **8₆** were calculated (Figure 3-2). The nanocube **3₆** and **6₆** have larger contact surface area of short intersurface distance (<1.5 Å) than **7₆** and **8₆**. As mentioned in Section 1.4.2, **3** and **6** have three methyl groups and three aromatic rings, whereas **7** lacks an aromatic ring and **8** possesses no methyl groups. These structural differences will reduce the contact surface, especially, of short intersurface distance. In other words, **7₆** and **8₆** possess not only smaller but also looser contact surfaces than **3₆** and **6₆**. Such loose contact surfaces should weaken their vdW forces and lower the association constants of **7₆** and **8₆**.

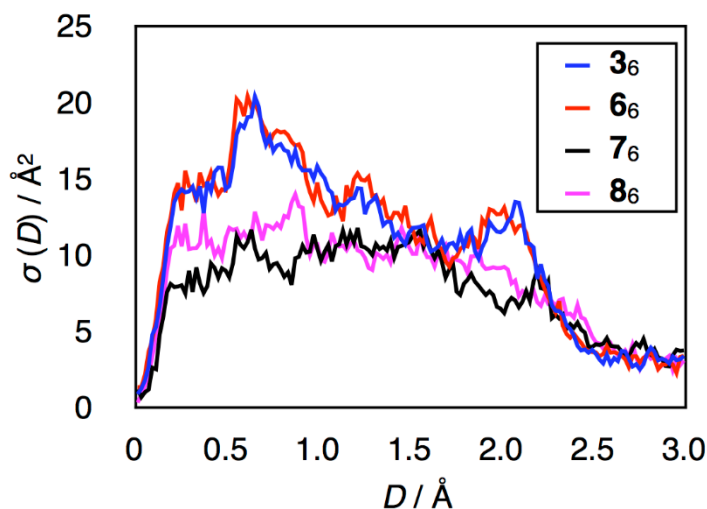


Figure 3-2. Intersurface distance distribution $\sigma(D)$ for **3₆**, **6₆**, **7₆**, and **8₆**.

The contact surface areas and the association constants of these nanocubes were also compared with other aqueous systems (Figure 3-3). The $\log_{10} K_a$ value and ΔS_{ASA} of the nanocubes, along with the average data of these two parameters of some categories of host-guest systems reported by Houk et al.,^[7] were plotted with the proportional relation mentioned in Section 1.5. The $\log_{10} K_a$ value of nanocube **3₆** and **6₆** is much larger than the value predicted from the ΔS_{ASA} and the proportional relation. Therefore this plot indicates enormously stronger vdW force per contact surface area of **3₆** and **6₆** than other host-guest systems.

3.3.3. Host-guest systems

To further consider the influence of the intersurface distance distribution, the relation between the structures and the reported association behaviors of host-guest systems with alpha-cyclodextrin (αCD)^[9] or cucurbit[7]uril (CB[7])^[10] (Figure 3-4a) was investigated. The crystal structures and association constants were collected from literatures (shown later in Table 3-3 and Table 3-4). The ΔS_{ASA} and the $\log_{10} K_a$ values of the host-guest complexes of αCD or CB[7] are calculated from the literatures and plotted in Figure 3-3. The plots for the αCD complexes relatively obey the proportional relation. Similar average values of ΔS_{ASA} and $\log_{10} K_a$ of the αCD complexes were also reported by Houk et al.^[7] On the other hand, the $\log_{10} K_a$ values of the CB[7] complexes with guest molecules **G1–G4** (Figure 3-4a) clearly surpass the

values expected from the relation. This large deviation implies that, in these systems, short intersurface distance strengthens their vdW force, resulting in the large $\log_{10} K_a$ values. To address this issue, the SAVPR method was performed for the host-guest complexes of α CD and CB[7]. The intersurface distance distribution of the four CB[7] systems is shown in Figure 3-4b. The order of the area of the contact surface of short intersurface distance (<2 Å) of these systems is **G1** ~ **G2** > **G3** > **G4**, which coincides with the order of the K_a values. The difference between **G4** and the other systems could be considered as the result of electrostatic interaction because **G4** possesses one positive charge while the others two. However, the difference between **G3** and **G1/G2** cannot be explained by electrostatic interaction. This result strongly indicates the correlation between the intersurface distance distribution $\sigma(D)$ and the association constant K_a of the systems. It should be noted that $\sigma(D)$ profiles of the α CD systems do not exhibit clear difference of the area of the contact surface of short intersurface distance, being consistent with the small dispersion of the association constants.

This analysis qualitatively demonstrates the importance of the intersurface distance of host-guest systems and the utility of the SAVPR method as a method to semiquantitatively compare the intersurface distance of supramolecular systems.

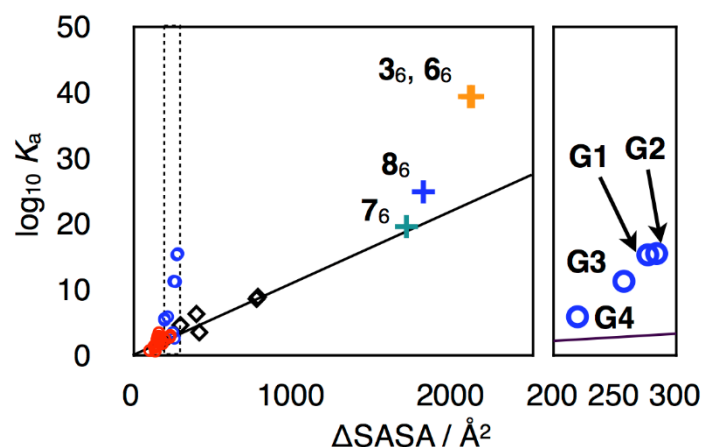


Figure 3-3. Plot of $\log_{10} K_a$ versus change of solvent-accessible surface area (ΔSASA). The green and blue crosshairs indicate **7₆** and **8₆** respectively. The orange crosshairs indicate **3₆** and **6₆** (they are overlapped). Red circles are the systems of α CD. Blue circles are the systems of CB[7]. Black diamonds are data reported by Houk et al. Black line corresponds to the proportional relation. For the nanocube systems, the MM-calculated contact surface areas and the experimental association constants were plotted. The plotted $\log_{10} K_a$ value of **3₆** and **6₆** is a lower limit. For the α CD and CB[7] systems, the crystal structures and the association constants in aqueous solution or buffer solution were plotted. For data by Houk et al., the reported values were plotted. The plot on the right side is a magnified view of the dashed rectangle of the left plot.

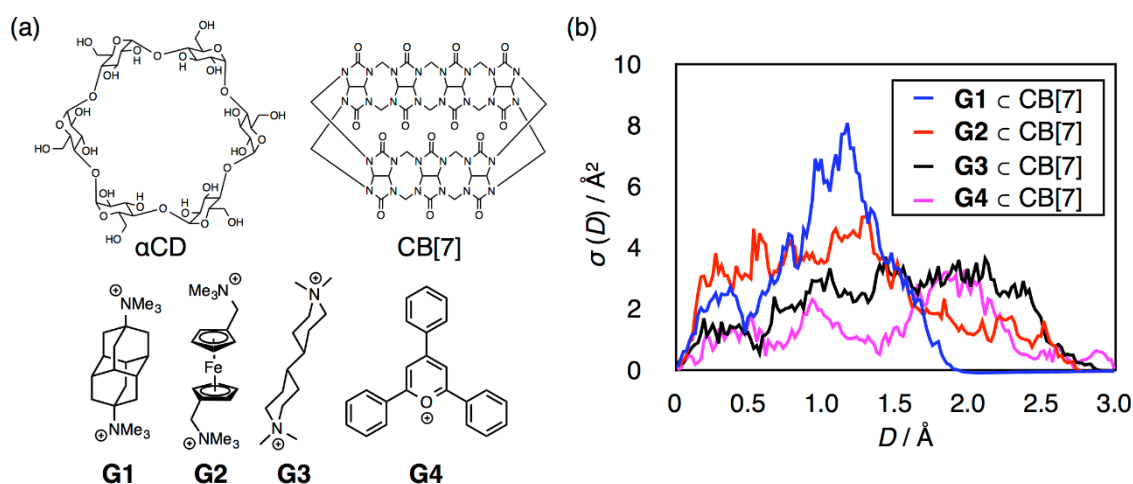


Figure 3-4. SAVPR analysis of CB[7] systems (a) The structures of hosts and selected four guests **G1–G4**; (b) Intersurface distance distribution $\sigma(D)$ for CB[7] systems.

3.4. Conclusion

The SAVPR method successfully provided a semiquantitative explanation for the wide dispersion of association constants of self-organizing systems with similar contact surface area.

Because of its ease, the SAVPR method is widely applicable to many other systems, especially to much large systems such as proteins. Such applications will offer further information about the systems and general knowledge of molecular interaction, promoting the research of supramolecular science and its application.

3.5. Detailed methods

Preparation of structures

The structures of nanocubes were optimized in AMBER 9 program package^[11] for **1₆** and **2₆** and in AMBER 14 program package^[12] for **3₆**, **6₆**, **7₆**, and **8₆**. Geometry optimization of **1₆** and **2₆** were conducted for isolated nanocubes, whereas those of the cationic nanocubes, **3₆**, **6₆**, **7₆**, and **8₆**, were conducted in the presence of water molecules and iodide ions. The total numbers of water molecules were 10915, 10914, 10930 and 10910 for **3₆**, **6₆**, **7₆**, and **8₆**, respectively, and the number of iodide ions was 12. Ten water molecules and one iodide ion were encapsulated in these nanocubes. For the nanocubes, the general AMBER force field (GAFF)^[13] and restrained electrostatic potential charges (RESP)^[14] based on the electrostatic potentials calculated with

the HF/6-31G(d)^[15] method, were employed. In the calculation of cationic nanocubes, TIP4P/Ew force field was also employed for water molecules and iodide ions. The crystal structures of **1**₆ and **3**₆ were adopted as the initial structures of the calculation of these nanocubes. The initial structure of **2**₆ was prepared by replacement of the substituent of **1**₆ and those of **6**₆, **7**₆, and **8**₆ were similarly derived from **3**₆, because of the unavailability of the crystal structure of these nanocubes. The structures of the monomers were generated by the dissociation of the corresponding nanocube in Materials Studio software (version 8.0; Biovia Inc., USA).

The structures of host-guest complexes were obtained from their crystal structures. All the crystal structures of host-guest complexes were obtained from CCDC database except one structure (**G27**⊂αCD), which was obtained from the original paper because its atomic coordinates are not available in CCDC. In some crystals, there are several different structures because of crystallographic independence or disorders of guest molecules. In such cases, all types of structures were adopted in principle. Some structures were complete and used without modification. The other structures needed modifications, or sometimes were abandoned, because of its incompleteness, especially (partial or total) lack of hydrogen atoms or minor disorder of OH or CH₂OH moiety of αCD host. Hydrogen atoms were attached manually to the atoms that lack hydrogen atom(s). The positions of these attached H atoms were optimized by means of MM calculation with COMPASS II force field in Materials Studio software. In this step, the other atoms, including the H atoms whose positions were specified by original data, were fixed. When OH or CH₂OH moiety of αCD host was found to be disordered, only one structure with higher occupancy was chosen and the other minor structure(s) was ignored. If occupancy was 0.50:0.50, this was chosen arbitrarily. This arbitral choice should not affect the estimation of surface areas because these minor disorders locate outside of the cavity of αCD host molecule in all cases.

Evaluation of surface areas

The calculations of surface areas were conducted by means of Materials Studio software. To evaluate the contact surface area of a complex, the structure of the dissociated form was prepared by dissociating the self-assembled complex in the software. Then the SASA of the

associated form and the dissociated form were calculated. The half value of the difference of these SASA (Δ SASA) was adopted as contact surface area, for the consistency with the report by Houk. The area of contact surface of a guest, which is used in the literature, can be approximated by the half value of the Δ SASA, which corresponds to the sum of the areas of contact surface of the guest and the host. This approximation holds when the contact surface areas of the host and the guest are close.

In our calculation, the radius of the probe sphere was set to 1.4 Å, which is the radius of the approximated sphere of a water molecule.

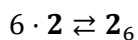
In the evaluation of SASA and Connolly surface areas, the default atomic radii of Materials Studio software, which correspond to the traditional values,^[16] were adopted. The actual values of these atomic radii are listed in Table 3-2.

Table 3-2. The list of atomic radii.

Element	Radius / Å	Element	Radius / Å
C	1.700	Cl	1.750
N	1.550	Br	1.850
H	1.200	I	1.980
O	1.520	Fe	1.260
S	1.800	Co	1.250
		Pt	1.750

Estimation of the upper limit of $K_a(2_6)$ and the lower limit of $K_a(3_6)$ and $K_a(6_6)$

We consider the hexamerization reaction of amphiphile **2**:



The total concentration of amphiphile **2** is referred to as c and the ratio of associated **2** to the total **2** molecules is referred to as ξ :

$$c = [\mathbf{2}] + 6[\mathbf{2}_6]$$

$$[\mathbf{2}] = (1 - \xi)c$$

$$[\mathbf{2}_6] = \frac{1}{6}\xi c$$

From these definitions, the association constant of **2**₆, $K_a(\mathbf{2}_6)$, can be expressed as

$$K_a(\mathbf{2}_6) = \frac{[\mathbf{2}_6]}{[\mathbf{2}]^6} = \frac{\xi c/6}{((1-\xi)c)^6} = \frac{\xi}{6(1-\xi)^6 c^5}$$

From the assumption that at most only 5% of amphiphile **2** assembled into nanocube in 2.0 mM solution, i.e., $c = 2.0$ mM and $\xi < 0.05$, we obtain

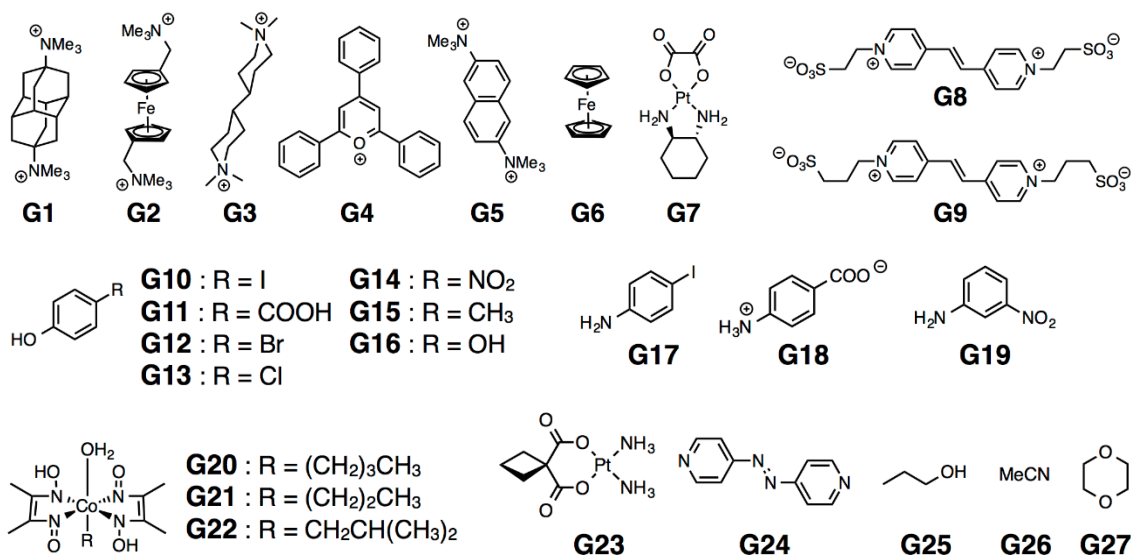
$$K_a(\mathbf{2}_6) < \frac{0.05}{6 \times 0.95^6 \times (2.0 \times 10^{-3} \text{ M})^5} = 3.54 \times 10^{11} \text{ M}^{-5}$$

The same equation and similar discussion apply to the case of **3**₆ and **6**₆ where too high association constants prevent the determination of these values. In the ITC measurement of **3**₆ and **6**₆, these aqueous solutions were diluted to $c = 2.3$ μM and the monomeric molecules, **3** and **6**, were not observed. From an assumption that at most only 1% of amphiphile **3** or **6** existed as monomers in 2.3 μM solution, i.e., $c = 2.3$ μM and $\xi > 0.99$, we obtain

$$K_a(\mathbf{3}_6), K_a(\mathbf{6}_6) > \frac{0.99}{6 \times 0.01^6 \times (2.3 \times 10^{-6} \text{ M})^5} = 2.56 \times 10^{39} \text{ M}^{-5}$$

Structures of selected host-guest complexes and their contact surface areas and association constants

In the following tables, “SASA(A)” and “SASA(D)” refer to the calculated SASA values of an associated and a dissociated form in \AA^2 , respectively. If some independent structures exist for a host-guest system, the average value was adopted. “CSA” is the contact surface area, which is the half value of ΔSASA , the difference of these two SASA values. “ $\log_{10} K_a$ ” is the common logarithm of its association constant K_a . For the system whose K_a values were reported by some groups, their median value for its K_a value was adopted.



Scheme 3-1. Structures of the selected guests, **G1–G9** for CB[7] and **G10–G27** for α CD.

Table 3-3. References of crystal structures and association constants of selected guests of CB[7].

	Crystal structure	Association constants
G1	Ref. 17	Ref. 17
G2	Ref. 18	Ref. 18
G3	Ref. 19	Ref. 19
G4	Ref. 20	Ref. 21
G5	Ref. 19	Ref. 19
G6	Ref. 22	Ref. 23
G7	Ref. 24	Ref. 24
G8	Ref. 25	Ref. 25
G9	Ref. 25	Ref. 25

Table 3-4. References of crystal structures and association constants of selected guests of α CD.

	Crystal structure	Association constants
G10	Ref.26	Ref.27
G11	Ref.28	Ref.29
G12	Ref.30	Ref.31
G13	Ref.32	Ref.31
G14	Ref.28	Ref.27,31,33,34,35,36,37,38
G15	Ref.32	Ref.31
G16	Ref.39	Ref.31,40
G17	Ref.41,42	Ref.43
G18	Ref.44	Ref.29,33
G19	Ref.45	Ref.29
G20	Ref.46	Ref.47
G21	Ref.47	Ref.47
G22	Ref.48	Ref.47
G23	Ref.49	Ref.50
G24	Ref.51	Ref.51
G25	Ref.52	Ref.53,54,55
G26	Ref.56	Ref.57
G27	Ref.58	Ref.57

Table 3-5. Surface areas and association constants of CB[7] systems.

	SASA(A)	SASA(D)	CSA	$\log_{10} K_a$	condition
G1	966.69	1520.34	276.82	15.30	D ₂ O buffered with CD ₃ COONa (50 mM), pH 4.74
G2	978.79	1546.73	283.97	15.50	aqueous solution, 25 °C
G3	966.54	1481.19	257.32	11.28	D ₂ O buffered with CD ₃ COONa (50 mM), pH 4.74
G4	1137.97	1577.10	219.57	5.88	aqueous solution, pH 1
G5	964.49	1503.69	269.60	11.23	D ₂ O buffered with CD ₃ COONa (50 mM), pH 4.74
G6	942.81	1343.15	200.17	>5.60	0.03 M TRIS buffer (pH 7.3) + 0.1 M NaCl
G7	1023.54	1424.69	200.58	5.36	TRIS buffer, pH 7.2, 25 °C
G8	1140.99	1646.13	252.57	3.5	D ₂ O–CD ₃ CN (10:1, v/v), 30 °C
G9	1187.36	1711.40	262.02	2.6	D ₂ O–CD ₃ CN (10:1, v/v), 30 °C

Table 3-6. Surface areas and association constants of α CD systems.

	SASA(A)	SASA(D)	CSA	$\log_{10} K_a$	condition ^[a]
G10	976.50	1303.69	163.60	2.94	
G11	989.41	1328.35	169.47	2.65	
G12	975.41	1287.93	156.26	2.85	phosphate buffer soln., pH 4.2, ionic strength of 0.18
G13	982.38	1287.84	152.73	2.47	phosphate buffer soln., pH 4.2, ionic strength of 0.18
G14	979.61	1304.84	162.61	2.02 ^[27]	
				2.30 ^[31]	
				2.10 ^[33]	phosphate buffer soln., pH 4.2, ionic strength of 0.18
				2.28 ^[34]	
				2.25 ^[35]	pH 6.8?
				2.21 ^[36]	10 mM sodium acetate solution, pH 4.3
				2.33 ^[37]	sodium formate buff. soln., pH 3.0, 0.1 M ionic strength
				2.31 ^[38]	
G15	992.38	1277.61	142.61	1.57	phosphate buffer soln., pH 4.2, ionic strength of 0.18
G16	995.38	1273.35	138.99	1.38 ^[31]	phosphate buffer soln., pH 4.2, ionic strength of 0.18
				0.92 ^[40]	distilled water soln.
G17	974.43	1304.10	164.84	3.45	0.05 M potassium hydrogenphosphthalate[sic] buffer
G18	964.38	1300.27	167.94	2.80 ^[29]	
				2.80 ^[33]	
G19	971.39	1303.86	166.24	1.87	
G20	1011.20	1482.63	235.72	3.03	
G21	1045.97	1509.63	231.83	2.72	
G22	1034.80	1491.66	228.43	2.56	
G23	1013.48	1387.98	187.25	1.77	
G24	982.87	1387.13	202.13	2.44	
G25	965.73	1234.68	134.48	1.36 ^[53]	
				1.46 ^[54]	
				1.43 ^[55]	
G26	959.74	1173.29	106.78	0.74	benzoic acid/benzoate buffer soln., pH 3.8 – 4.5
G27	949.49	1233.49	142.00	0.65	benzoic acid/benzoate buffer soln., pH 3.8 – 4.5

^[a] All of the experiments were conducted in an aqueous solution at the temperature or 25 °C.

Intersurface distance densities of host-guest complexes

Here, the intersurface distance distributions $\sigma(D)$ of host-guest complexes are shown. If a complex has some independent structures in its crystal, $\sigma(D)$ of all of the structures are shown. As mentioned above, the K_a values of the host-guest complexes have a positive correlation with the areas of the contact surfaces of short intersurface distance ($<2 \text{ \AA}$). In almost all the cases, the different structures of a complex have a similar $\sigma(D)$ profile.

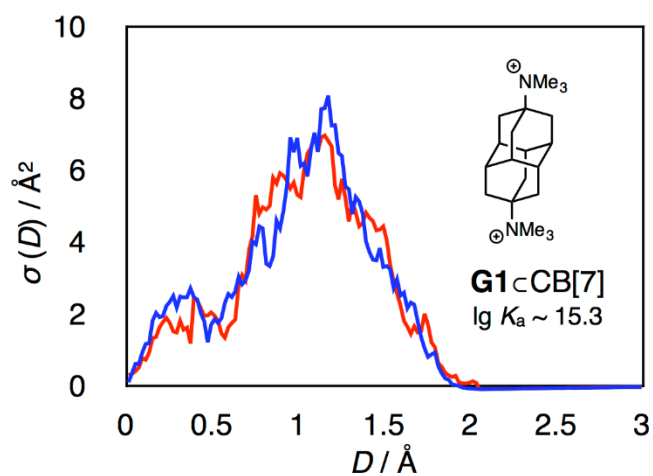


Figure 3-5. $\sigma(D)$ for **G1** in **CB[7]**.

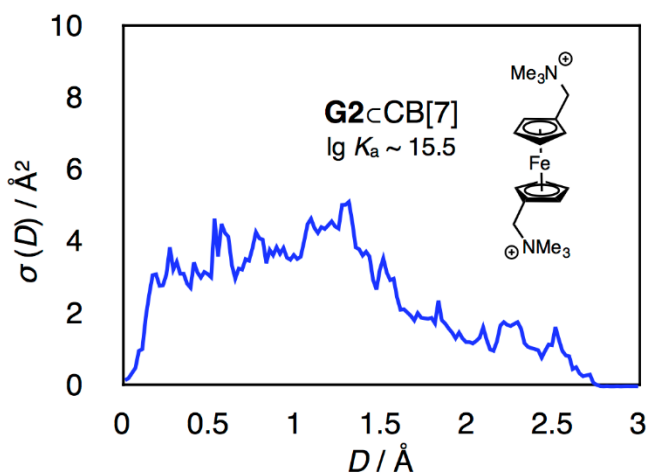


Figure 3-6. $\sigma(D)$ for **G2** in **CB[7]**.

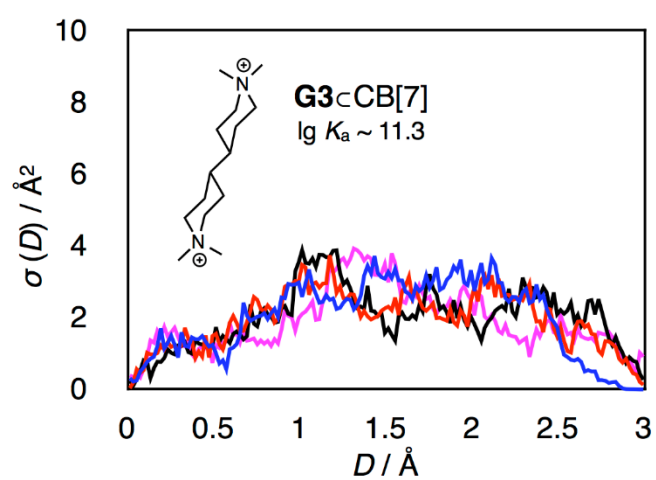


Figure 3-7. $\sigma(D)$ for G3C[7].

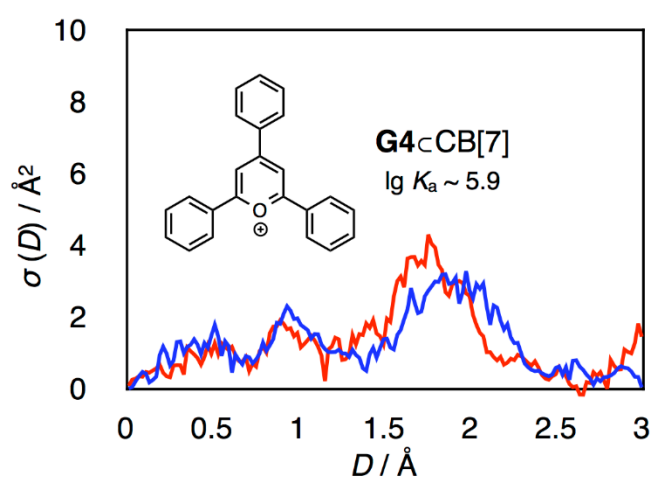


Figure 3-8. $\sigma(D)$ for G4C[7].

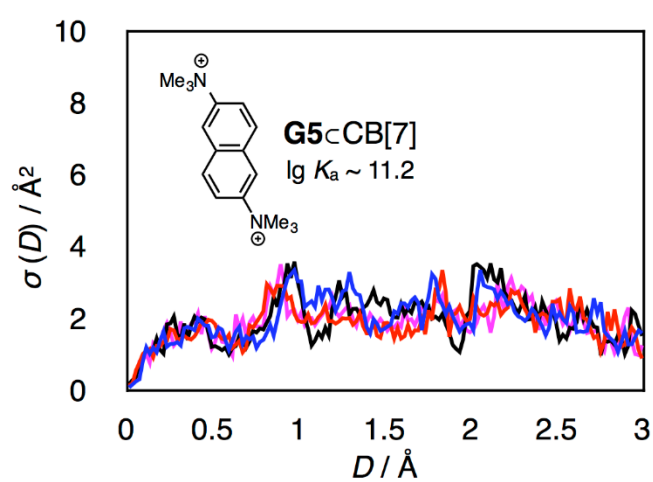


Figure 3-9. $\sigma(D)$ for G5C[7].

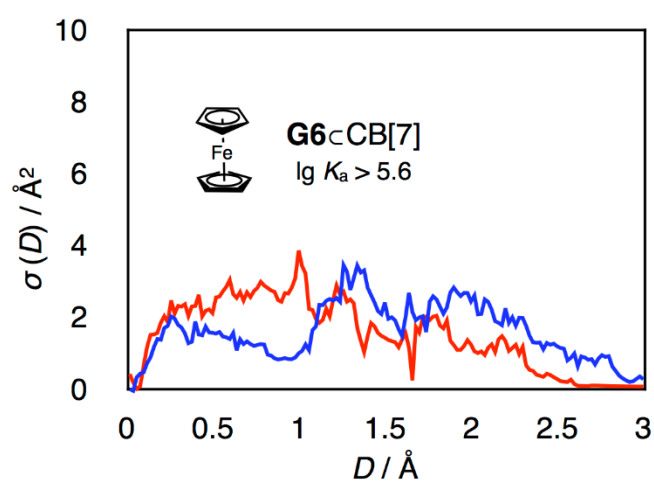


Figure 3-10. $\sigma(D)$ for $\text{G6}@\text{CB}[7]$.

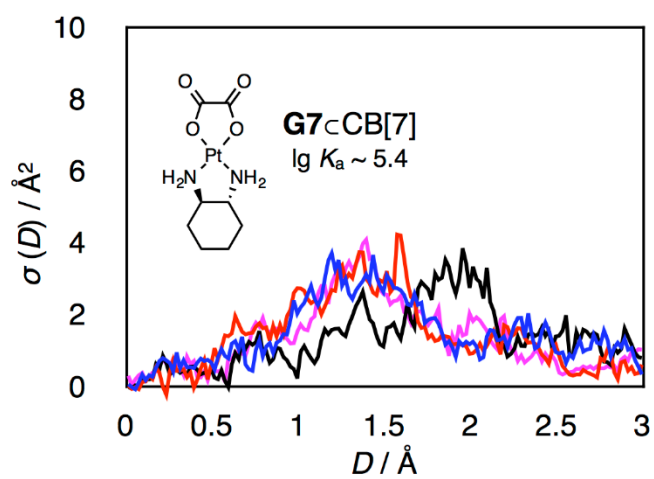


Figure 3-11. $\sigma(D)$ for $\text{G7}@\text{CB}[7]$.

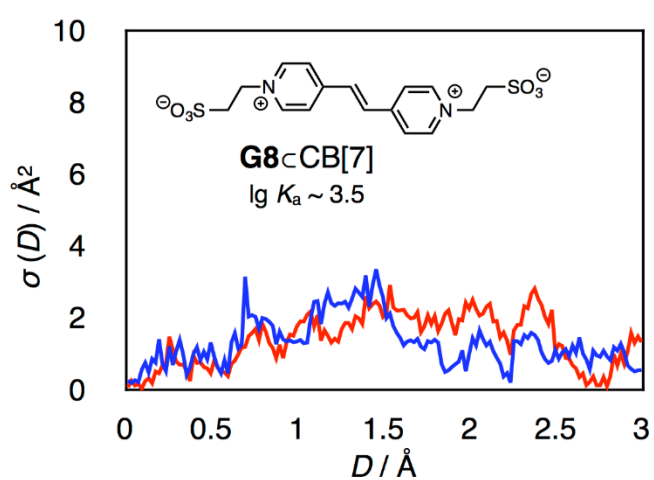


Figure 3-12. $\sigma(D)$ for $\text{G8}@\text{CB}[7]$.

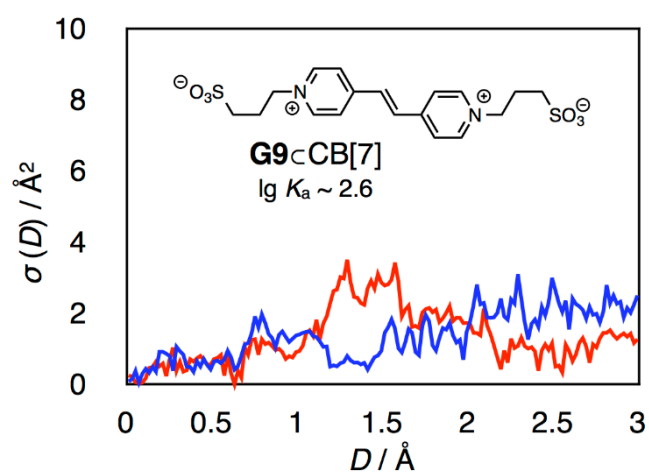


Figure 3-13. $\sigma(D)$ for G9C[CB[7]].

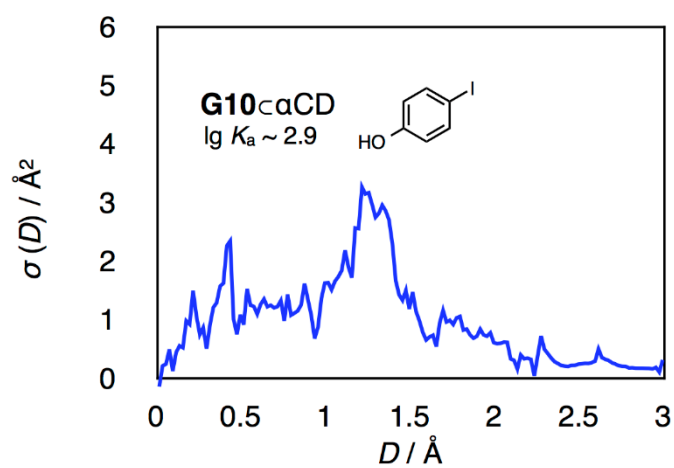


Figure 3-14. $\sigma(D)$ for G10C[α CD].

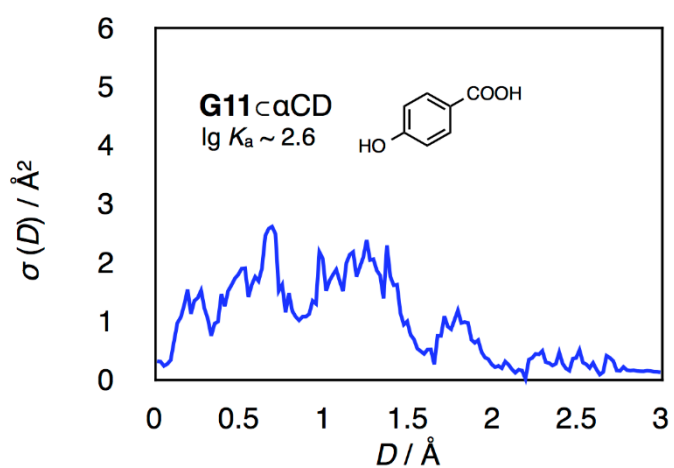


Figure 3-15. $\sigma(D)$ for G11C[α CD].

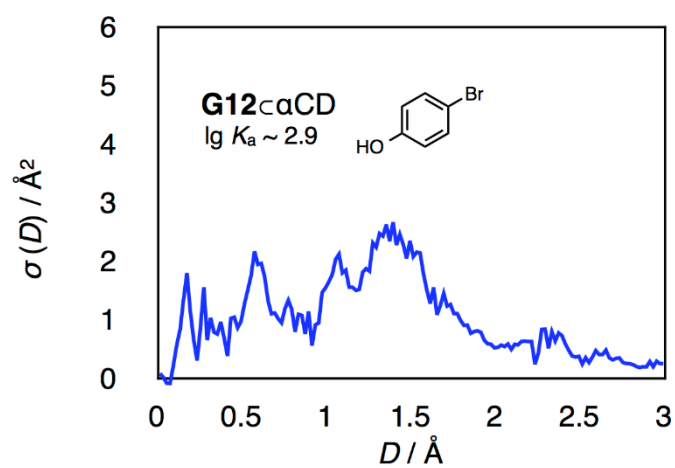


Figure 3-16. $\sigma(D)$ for **G12 \subset α CD**.

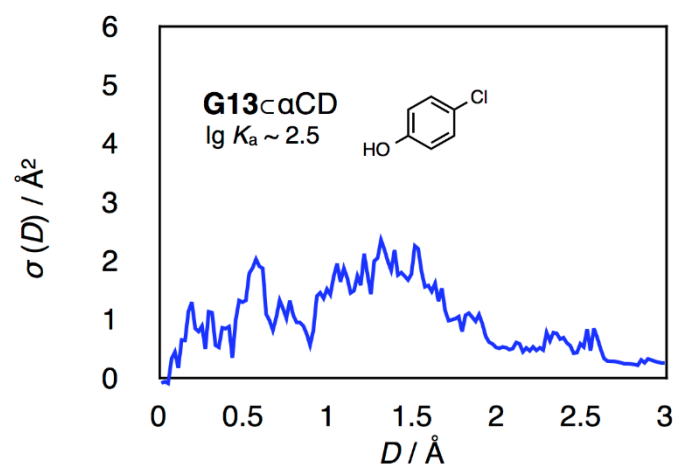


Figure 3-17. $\sigma(D)$ for **G13 \subset α CD**.

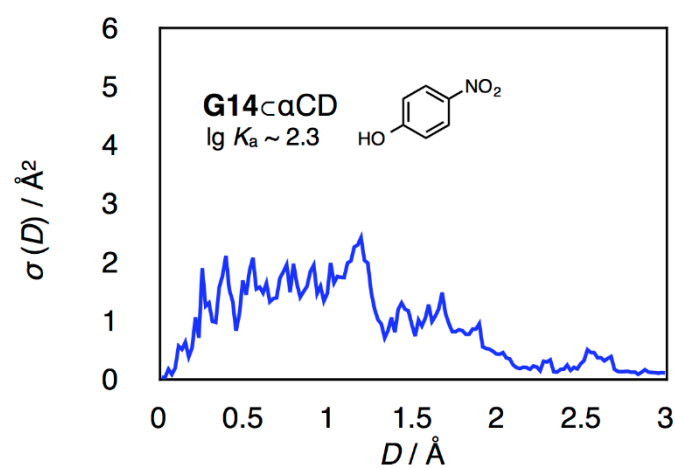


Figure 3-18. $\sigma(D)$ for **G14 \subset α CD**.

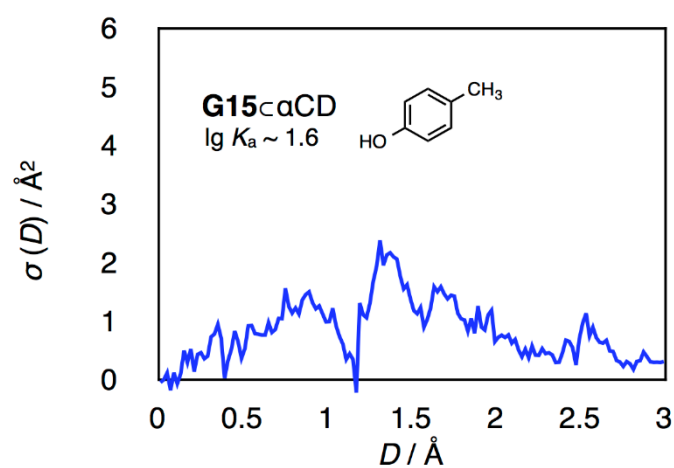


Figure 3-19. $\sigma(D)$ for G15 α CD.

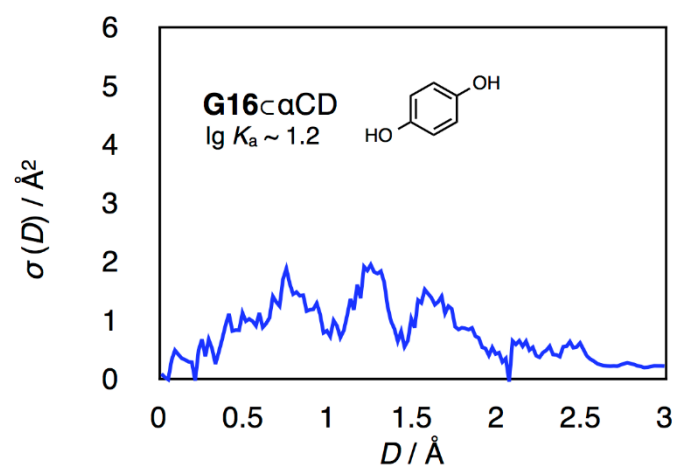


Figure 3-20. $\sigma(D)$ for G16 α CD.

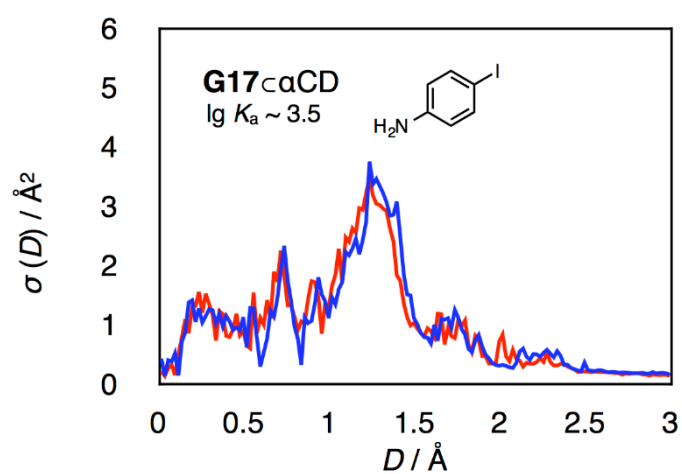


Figure 3-21. $\sigma(D)$ for G17 α CD.

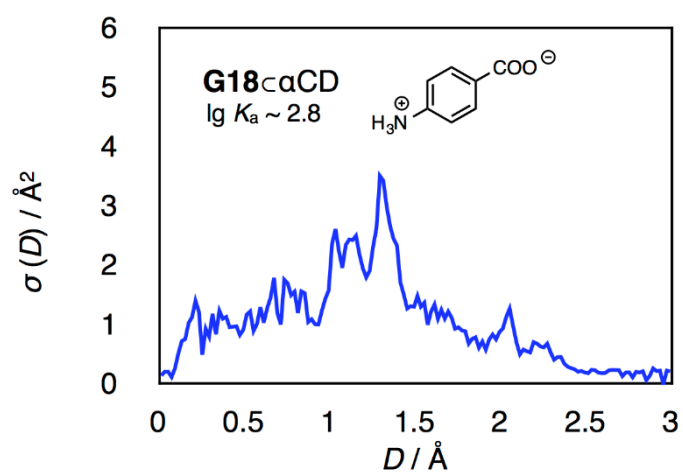


Figure 3-22. $\sigma(D)$ for G18 α CD.

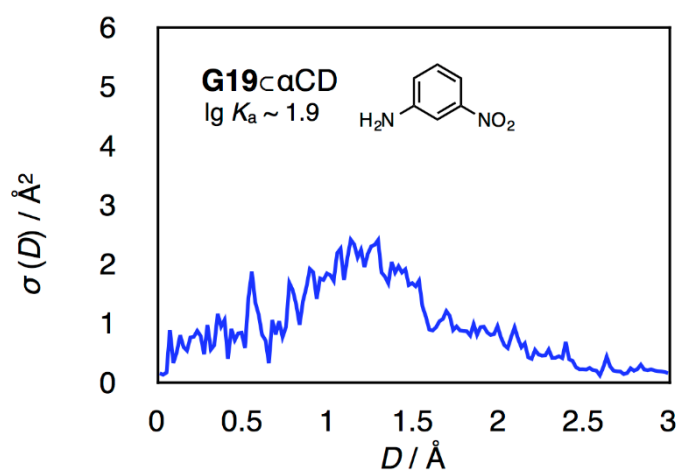


Figure 3-23. $\sigma(D)$ for G19 α CD.

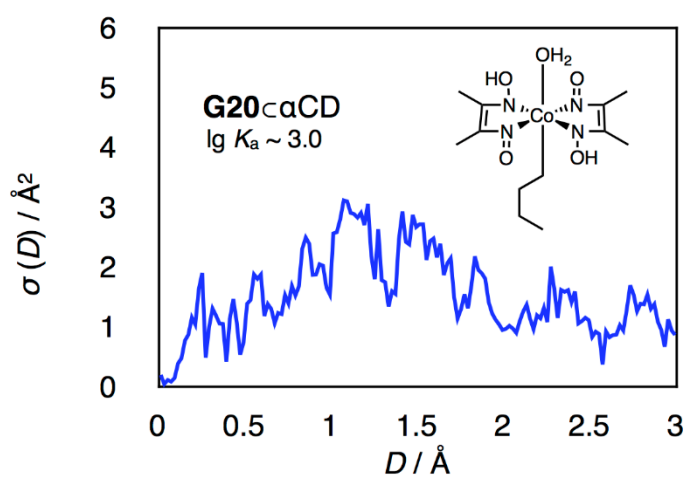


Figure 3-24. $\sigma(D)$ for G20 α CD.

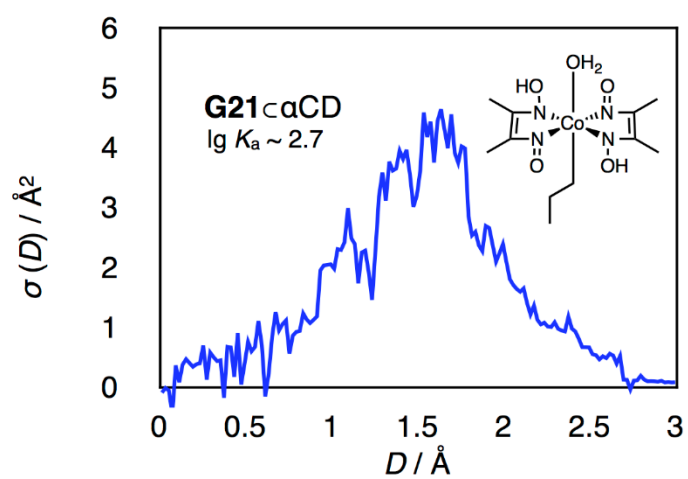


Figure 3-25. $\sigma(D)$ for **G21**⊂αCD.

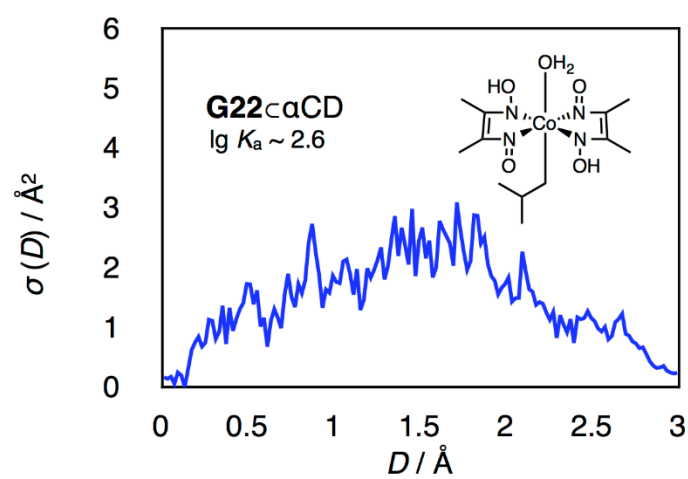


Figure 3-26. $\sigma(D)$ for **G22**⊂αCD.

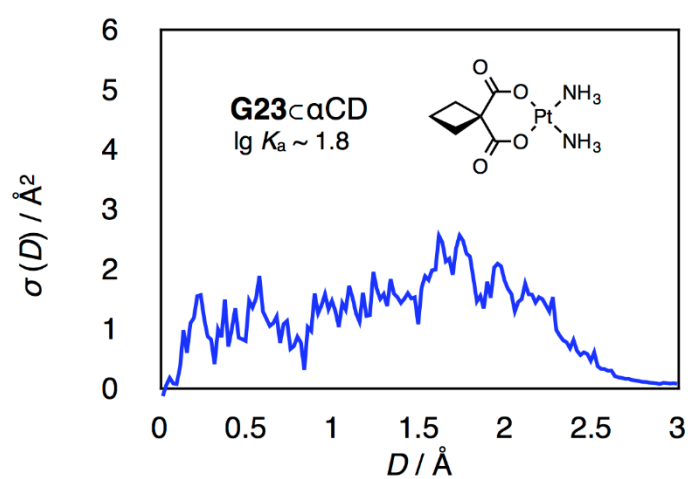


Figure 3-27. $\sigma(D)$ for **G23**⊂αCD.

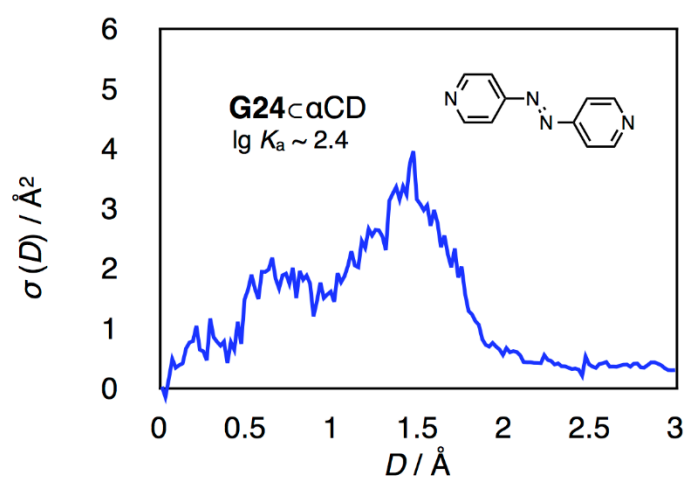


Figure 3-28. $\sigma(D)$ for G24⊂αCD.

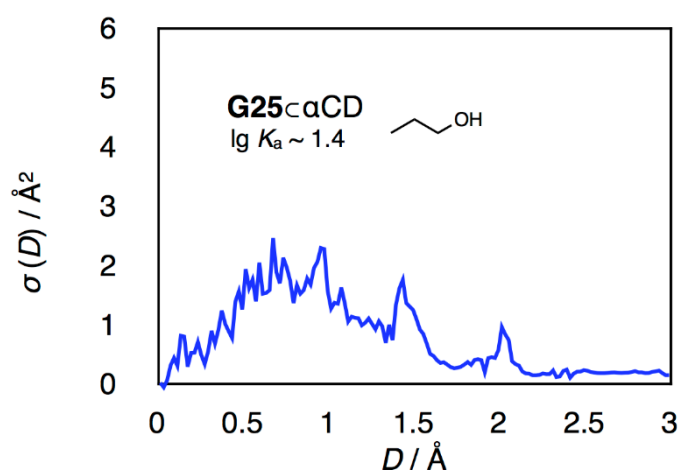


Figure 3-29. $\sigma(D)$ for G25⊂αCD.

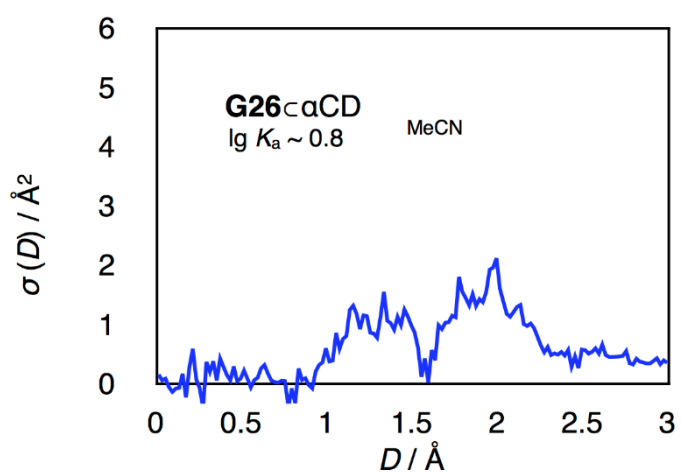


Figure 3-30. $\sigma(D)$ for G26⊂αCD.

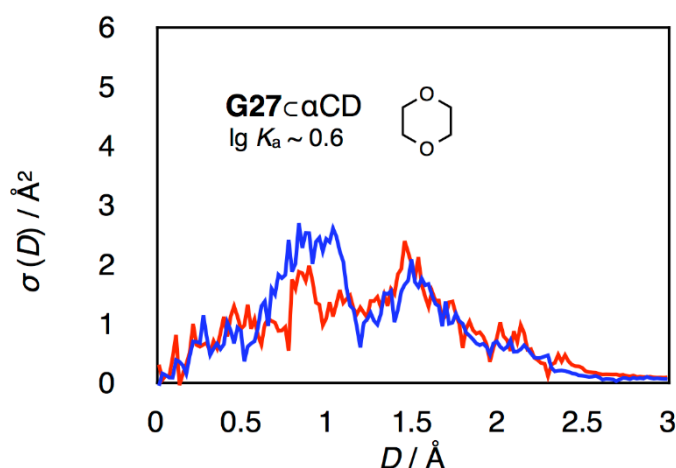


Figure 3-31. $\sigma(D)$ for G27-cyclodextrin.

References and Notes

- ¹ Tanaka, N.; Zhan, Y.-Y.; Ozawa, Y.; Kojima, T.; Koide, T.; Mashiko, T.; Nagashima, U.; Tachikawa, M.; Hiraoka, S. *Chem. Commun.* 2018, Advance Article. (DOI: 10.1039/C8CC00695D)
- ² a) Maibaum, L.; Dinner, A. R.; Chandler, D. *J. Phys. Chem. B* **2004**, *108*, 6778–6781; b) Tanford, C. *The Hydrophobic Effect: Formation of Micelles and Biological Membranes*; Wiley: New York, 1973.
- ³ a) Dill, K. A. *Biochemistry* **1990**, *29*, 7133–7155; b) Levy, Y.; Onuchic, J. N. *Annu. Rev. Biophys. Biomol. Struct.* **2006**, *35*, 389–415; c) Kauzmann, W. *Adv. Protein Chem.* **1959**, *14*, 1–63.
- ⁴ a) Breiten, B.; Lockett, M. R.; Sherman, W.; Fujita, S.; Al-Sayah, M.; Lange, H.; Bowers, C. M.; Heroux, A.; Krilov, G.; Whitesides, G. M. *J. Am. Chem. Soc.* **2013**, *135*, 15579–15584; b) Snyder, P. W.; Mecnovic, J.; Moustakas, D. T.; Thomas, S. W. 3rd.; Harder, M.; Mack, E. T.; Lockett, M. R.; Héroux, A.; Sherman, W.; Whitesides, G. M. *Proc. Natl. Acad. Sci. U. S. A.* **2011**, *108*, 17889–17894; c) Snyder, P. W.; Lockett, M. R.; Moustakas, D. T.; Whitesides, G. M. *Eur. Phys. J. Special Topics* **2014**, *223*, 853–891.
- ⁵ a) Nitschke, J. R.; Hutin, M.; Bernardinelli, G. *Angew. Chem., Int. Ed.* **2004**, *43*, 6724–6727; b) Gibb, C. L. D.; Gibb, B. C. *Chem. Commun.* **2007**, 1635–1637; c) Gibb, C. L. D.; Gibb, B. C. *J. Am. Chem. Soc.* **2004**, *126*, 11408–11409; d) Ryu, J.-H.; Hong, D.-J.; Lee, M. *Chem. Commun.* **2008**, 1043–1054; e) Besenius, P.; Portale, G.; Bomans, P. H. H.; Janssen, H. M.; Palmans, A. R. A.; Meijer, E. W. *Proc. Natl. Acad. Sci. U. S. A.* **2010**, *107*, 17888–17893; f) Malakoutikhah, M.; Peyralans, J. J.-P.; Colomb-Delsuc, M.; Fanlo-Virgós, H.; Stuart, M. C. A.; Otto, S. *J. Am. Chem. Soc.* **2013**, *135*, 18406–18417; g) Li, H.; Zhang, H.; Lammer, A. D.; Wang, M.; Li, X.; Lynch, V. M.; Sessler, J. L. *Nat. Chem.* **2015**, *7*, 1003–1008.
- ⁶ a) Inouye, M.; Fujimoto, K.; Furusyo, M.; Nakazumi, H. *J. Am. Chem. Soc.* **1999**, *121*, 1452–1458; b) Mal, P.; Schultz, D.; Beyeh, K.; Rissanen, K.; Nitschke, J. R. *Angew. Chem., Int. Ed.* **2008**, *47*, 8297–8301; c) Hooley, R. J.; Van Anda, H. J.; Rebek, J. Jr. *J. Am. Chem. Soc.* **2007**, *129*, 13464–13473; d) Biro, S. M.; Bergman, R. G.; Raymond, K. N. *J. Am. Chem. Soc.*, **2007**, *129*, 12094–12095.
- ⁷ Houk, K. N.; Leach, A. G.; Kim, S. P.; Zhang, X. *Angew. Chem., Int. Ed.* **2003**, *42*, 4872–4897.
- ⁸ Matsumoto, S.; Iwamoto, H.; Mizutani, T. *Chem. Asian. J.* **2010**, *5*, 1163–1170.
- ⁹ a) Li, S.; Purdy, W. C. *Chem. Rev.* **1992**, *92*, 1457–1470; b) Dodziuk, H. *Cyclodextrins and Their Complexes: Chemistry, Analytical Methods, Applications*; Wiley-VCH: Weinheim, Germany, 2006; c) *Cyclodextrins*; Szejtli, J.; Osa, T., Eds.; Comprehensive Supramolecular

Chemistry, Vol. 3; Elsevier: Oxford, 1996.

¹⁰ a) Lagona, J.; Mukhopadhyay, P.; Chakrabarti, S.; Isaacs, L. *Angew. Chem., Int. Ed.* **2005**, *44*, 4844–4870; b) Lee, J. W.; Samal, S.; Selvapalam, N.; Kim, H.-J.; Kim, K. *Acc. Chem. Res.* **2003**, *36*, 621–630.

¹¹ Case D.A.; Darden, T.A.; Cheatham, T. E. III.; Simmerling, C. L.; Wang, J.; Duke, R. E.; Luo, R.; Merz, K. M.; Pearlman, D. A.; Crowley, M.; Walker, R. C.; Zhang, W.; Wang, B.; Hayik, S.; Roitberg, A.; Seabra, G.; Wong, K. F.; Paesani, F.; Wu, X.; Brozell, S.; Tsui, V.; Gohlke, H.; Yang, L.; Tan, C.; Mongan, J.; Hornak, V.; Cui, G.; Beroza, P.; Mathews, D. H.; Schafmeister, C.; Ross, W. S.; Kollman P. A. AMBER 9, University of California, San Francisco, 2006.

¹² Case, D. A.; Babin, V.; Berryman, J. T.; Betz, R. M.; Cai, Q.; Cerutti, D. S.; Cheatham, T. E., III.; Darden, T. A.; Duke, R. E.; Gohlke, H.; Goetz, A. W.; Gusarov, S.; Homeyer, N.; Janowski, P.; Kaus, J.; Kolossváry, I.; Kovalenko, A.; Lee, T. S.; LeGrand, S.; Luchko, T.; Luo, R.; Madej, B.; Merz, K. M.; Paesani, F.; Roe, D. R.; Roitberg, A.; Sagui, C.; Salomon-Ferrer, R.; Seabra, G.; Simmerling, C. L.; Smith, W.; Swails, J.; Walker, R. C.; Wang, J.; Wolf, R. M.; Wu, X.; Kollman, P. A. AMBER 14, University of California, San Francisco, 2014.

¹³ Wang, J. M.; Wolf, R. M.; Caldwell, J. W.; Kollman, P. A.; Case, D. A. *J. Comput. Chem.* **2004**, *25*, 1157–1174.

¹⁴ Bayly, C. I.; Cieplak, P.; Cornell, W.; Kollman, P. A. *J. Phys. Chem.* **1993**, *97*, 10269–10280.

¹⁵ Frisch, M. J.; Trucks, G. W.; Schlegel, H. B.; Scuseria, G. E.; Robb, M. A.; Cheeseman, J. R.; Scalmani, G.; Barone, V.; Petersson, G. A.; Nakatsuji, H.; Li, X.; Caricato, M.; Marenich, A.; Bloino, J.; Janesko, B. G.; Gomperts, R.; Mennucci, B.; Hratchian, H. P.; Ortiz, J. V.; Izmaylov, A. F.; Sonnenberg, J. L.; Williams-Young, D.; Ding, F.; Lipparini, F.; Egidi, F.; Goings, J.; Peng, B.; Petrone, A.; Henderson, T.; Ranasinghe, D.; Zakrzewski, V. G.; Gao, J.; Rega, N.; Zheng, G.; Liang, W.; Hada, M.; Ehara, M.; Toyota, K.; Fukuda, R.; Hasegawa, J.; Ishida, M.; Nakajima, T.; Honda, Y.; Kitao, O.; Nakai, H.; Vreven, T.; Throssell, K.; Montgomery, J. A., Jr.; Peralta, J. E.; Ogliaro, F.; Bearpark, M.; Heyd, J. J.; Brothers, E.; Kudin, K. N.; Staroverov, V. N.; Keith, T.; Kobayashi, R.; Normand, J.; Raghavachari, K.; Rendell, A.; Burant, J. C.; Iyengar, S. S.; Tomasi, J.; Cossi, M.; Millam, J. M.; Klene, M.; Adamo, C.; Cammi, R.; Ochterski, J. W.; Martin, R. L.; Morokuma, K.; Farkas, O.; Foresman, J. B.; Fox, D. J. Gaussian, Inc., Wallingford CT, 2016.

¹⁶ Bondi, A. *J. Phys. Chem.* **1964**, *68*, 441–451.

¹⁷ Cao, L.; Šekutor, M.; Zavalij, P. Y.; Mlinarić-Majerski, K.; Glaser, R.; Isaacs, L. *Angew. Chem., Int. Ed.* **2014**, *53*, 988–993.

¹⁸ Rekharsky, M. V.; Mori, T.; Yang, C.; Ko, Y. H.; Selvapalam, N.; Kim, H.; Sobransingh, D.; Kaifer, A. E.; Liu, S.; Isaacs, L.; Chen, W.; Moghaddam, S.; Gilson, M. K.; Kim, K.; Inoue, Y. *Proc. Natl. Acad. Sci. U.S.A.* **2007**, *104*, 20737–20742.

¹⁹ Cao, L.; Škalamera, Đ.; Zavalij, P. Y.; Hostaš, J.; Hobza, P.; Mlinarić-Majerski, K.; Glaser, R.; Isaacs, L. *Org. Biomol. Chem.* **2015**, *13*, 6249–6254.

²⁰ Montes-Navajas, P.; Garcia, H. *J. Phys. Chem. C* **2010**, *114*, 2034–2038.

²¹ Montes-Navajas, P.; Teruel, L.; Corma, A.; Garcia, H. *Chem. Eur. J.* **2008**, *14*, 1762–1768.

²² Jeon, W. S.; Moon, K.; Park, S. H.; Chun, H.; Ko, Y. H.; Lee, J. Y.; Lee, E. S.; Samal, S.; Selvapalam, N.; Rekharsky, M. V.; Sindelar, V.; Sobransingh, D.; Inoue, Y.; Kaifer, A. E.; Kim, K. *J. Am. Chem. Soc.* **2005**, *127*, 12984–12989.

²³ Ong, W.; Kaifer, A. E. *Organometallics* **2003**, *22*, 4181–4183.

²⁴ Jeon, Y. J.; Kim, S.-Y.; Ko, Y. H.; Sakamoto, S.; Yamaguchi, K.; Kim, K. *Org. Biomol. Chem.* **2005**, *3*, 2122–2125.

²⁵ Vedernikov, A. I.; Lobova, N. A.; Kuz'mina, L. G.; Howard, J. A. K.; Strelenko, Y. A.; Alfimov, M. V.; Gromov, S. P. *J. Mol. Struct.* **2011**, *989*, 114–121.

²⁶ Harata, K. *Carbohydr. Res.* **1976**, *48*, 265–270.

²⁷ Rüdiger, V.; Eliseev, A.; Simova, S.; Schneider, H.-J.; Blandamer, M. J.; Cullis, P. M.; Meyer,

- A. J. *J. Chem. Soc., Perkin Trans. 2* **1996**, 2119–2123.
- ²⁸ Harata, K. *Bull. Chem. Soc. Jpn.* **1977**, *50*, 1416–1424.
- ²⁹ Harata, K. *Bioorg. Chem.* **1981**, *10*, 255–265.
- ³⁰ Kamitori, S.; Toyama, Y.; Matsuzaka, O. *Carbohydr. Res.* **2001**, *332*, 235–240.
- ³¹ Bertrand, G. L.; Faulkner, J. R.; Han, S. M.; Armstrong, D. W. *J. Phys. Chem.* **1989**, *93*, 6863–6867.
- ³² Muraoka, S.; Matsuzaka, O.; Kamitori, S.; Okuyama, K. *Carbohydr. Res.* **1999**, *320*, 261–266.
- ³³ Lewis, E. A.; Hansen, L. D. *J. Chem. Soc., Perkin Trans. 2* **1973**, 2081–2085.
- ³⁴ Gelb, R. I.; Schwartz, L. M.; Cardelino, B.; Laufer, D. A. *Anal. Biochem.* **1980**, *103*, 362–368.
- ³⁵ Korpela, T. K.; Himanen, J.-P. *J. Chromatogr.* **1984**, *290*, 351–361.
- ³⁶ Eftink, M. R.; Harrison, J. C. *Bioorg. Chem.* **1981**, *10*, 388–398.
- ³⁷ Harata, K. *Bull. Chem. Soc. Jpn.* **1978**, *51*, 2737–2738.
- ³⁸ Harata, K. *Bioorg. Chem.* **1980**, *9*, 530–539.
- ³⁹ Steiner, T.; Saenger, W. *Carbohydr. Lett.* **1994**, *1*, 143–150.
- ⁴⁰ Siimer, E.; Kõbu, M.; Kurvits, M. *Thermochim. Acta* **1990**, *170*, 89–95.
- ⁴¹ Saenger, W.; Beyer, K.; Manor, P. C. *Acta Cryst.* **1976**, *B32*, 120–128.
- ⁴² Harata, K. *Bull. Chem. Soc. Jpn.* **1975**, *48*, 2409–2413.
- ⁴³ Gelb, R. I.; Schwartz, L. M.; Laufer, D. A. *Carbohydr. Res.* **1983**, *118*, 111–117.
- ⁴⁴ Elasaad, K.; Norberg, B.; Wouters, J. *Supramol. Chem.* **2012**, *24*, 312–324.
- ⁴⁵ Harata, K. *Bull. Chem. Soc. Jpn.* **1980**, *53*, 2782–2786.
- ⁴⁶ Chen, Y.; Luo, L.-B.; Chen, H.-L.; Hu, C.-H.; Chen, J.; Zhen, P.-J. *Bull. Chem. Soc. Jpn.* **2000**, *73*, 1375–1378.
- ⁴⁷ Luo, L. B.; Chen, H. L.; Tang, W. X.; Zhang, Z. Y.; Mak, T. C. W. *J. Chem. Soc., Dalton Trans.* **1996**, 4425–4430.
- ⁴⁸ Luo, L.-B.; Chen, Y.; Chen, H.-L.; Zhang, Z.-Y.; Zhou, Z.-Y.; Mak, T. C. W. *Inorg. Chem.* **1998**, *37*, 6147–6152.
- ⁴⁹ Alston, D. R.; Slawin, A. M. Z.; Stoddart, J. F.; Williams, D. J. *J. Chem. Soc., Chem. Commun.* **1985**, 1602–1604.
- ⁵⁰ Alston, D. R.; Aston, P. R.; Lilley, T. H.; Stoddart, F.; Zarzycki, R. *Carbohydr. Res.* **1989**, *192*, 259–281.
- ⁵¹ Gu, Z.-Y.; Guo, D.-S.; Liu, Y. *Carbohydr. Res.* **2010**, *345*, 2670–2675.
- ⁵² Saenger, W.; McMullan, R. K.; Fayos, J.; Mootz, D. *Acta Cryst.* **1974**, *B30*, 2019–2028.
- ⁵³ Hallén, D.; Schön, A.; Shehatta, I.; Wadsö, I. *J. Chem. Soc., Faraday Trans.* **1992**, *88*, 2859–2863.
- ⁵⁴ Fujiwara, H.; Arakawa, H.; Murata, S.; Sasaki, Y. *Bull. Chem. Soc. Jpn.* **1987**, *60*, 3891–3894.
- ⁵⁵ Barone, G.; Castronuovo, G.; Del Vecchio, P.; Elia, V.; Muscetta, M. *J. Chem. Soc., Faraday Trans. 1* **1986**, *82*, 2089–2101.
- ⁵⁶ Aree, T.; Jacob, J.; Saenger, W.; Hoier, H. *Carbohydr. Res.* **1998**, *307*, 191–197.
- ⁵⁷ Gelb, R. I.; Schwartz, L. M.; Radeods, M.; Edmonds, R. B.; Laufer, D. A. *J. Am. Chem. Soc.* **1982**, *104*, 6283–6288.
- ⁵⁸ Ceborska, M. *J. Carbohydr. Chem.* **2014**, *33*, 48–53.

Chapter 4.

Effect of Small Structural Difference on Self-Assembly

In previous sections, the importance of weak intermolecular interactions and the applicability of the SAVPR method were explained. This section introduces another example of application of the SAVPR method. To further investigate the effect of the methyl groups on the association behavior of nanocubes, a novel hexaphenylbenzene derivative **9**, which bears only two methyl groups, was synthesized. An attempt to obtain the nanocube **9**₆ resulted in an unidentifiable mixture. The SAVPR method provided some possibilities about the constituent in the mixture.

4.1. Introduction

In natural systems, intermolecular interactions such as van der Waals (vdW) force and the solvophobic effect, especially the hydrophobic effect, play an important role in their self-assembly phenomena.^[1] Artificial supramolecular systems also exploit these interactions.^[2] The formation of complex structures by these effects requires delicate molecular design; as small difference as only one methyl group can become essential. For example, two amino acids whose difference is only one methyl group, such as serine/threonine and valine/isoleucine, are differently employed in proteins. These differences become very important in some cases such as activity of antifreeze polypeptide^[3] and abnormal production of amyloid beta peptide which cause familial Alzheimer's disease.^[4] Some artificial host-guest systems change their association behavior according to the small difference of the structure of guests, such as one methyl group or one methylene group.^[5] Another example where small structural difference of components is important is nanocube.^[6,7,8] Hexaphenylbenzene derivative **1** hexamerizes into nanocube **1**₆ in methanol/water solution whereas its analog **2** does not (Figure 4-1). In the previous chapter, this difference has been explained by the strength of intermolecular interactions that is affected by the detailed structures of contact surfaces. The nanocube **1**₆ should be stabilized by the vdW force between the closely contacted methyl groups, while **2**₆ would not enjoy such stabilization. Such phenomena were also observed in cationic nanocubes, **3**₆, **6**₆, **7**₆, and **8**₆; the ratio of their association affinities cannot be explained only by difference of contact surface areas but that of the detailed structures of contact surfaces should also

contribute.

In this chapter, another analog **9**, where **1** is deprived of only one methyl group, was synthesized and its association behavior was investigated. The comparison of the association behaviors of **1** and **9** will offer the information about the effect of one methyl group on the formation of the nanocube and the driving force of the association: vdW force and the hydrophobic effect..

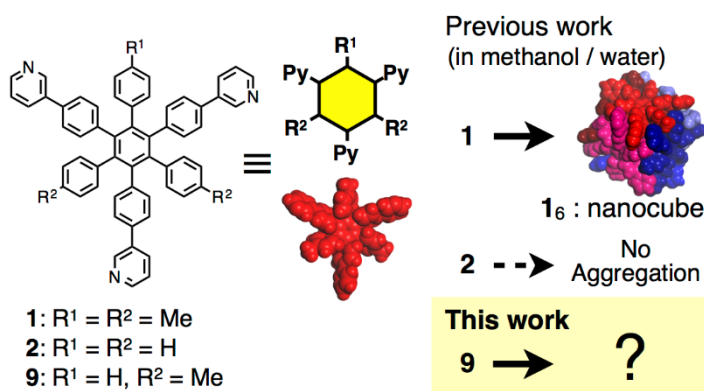


Figure 4-1. Structure of **1**, **2**, and **9** and their association behavior into nanocube.

4.2. Structural consideration: possible isomers of the nanocube

Before experiments, the possible structures of nanocube **9₆** are discussed. Nanocube **9₆** is an analog of nanocube **1₆** (a schematic illustration is shown in Figure 4-2). **1₆** possesses a six-fold rotation-reflection (S_6) axis. Around the axis, six methyl groups exist. Hereafter the positions of these methyl groups are referred to as “polar”, using an analogy from the Earth. Besides these six methyl groups, two kinds of methyl group exist and the number of each of them is six in a nanocube. The positions of these twelve methyl groups are referred to as “equatorial”. The isomers of **9₆** have the structures where one methyl group of each monomer molecule in **1₆** is replaced with a hydrogen atom. These isomers are named according to the structures of two sets of three monomers. These sets are referred to as “northern hemisphere” and “southern hemisphere”. These two hemispheres possess eleven isomers, to which **A–K** were assigned as a name. By the combination of the hemispheres, 138 geometrical isomers of **9₆** were classified (for the detail of counting and nomenclature of isomers, see Section 4.5). Because the investigation of all of the isomers is not realistic, the following six isomers, which have

characteristic combinations of the number of methyl groups of different types, are selected and investigated (Figure 4-3). Isomer **GG** lacks all of the polar methyl groups. **FG** and **GH** lack five polar methyl groups and one equatorial methyl group. **AA**, **DD**, and **AD** lack six equatorial methyl groups. These 138 isomers of **9₆** can differ in the formation Gibbs energies because of the difference of their contact surfaces. This preference may cause selective formation of a few kinds of the isomers.

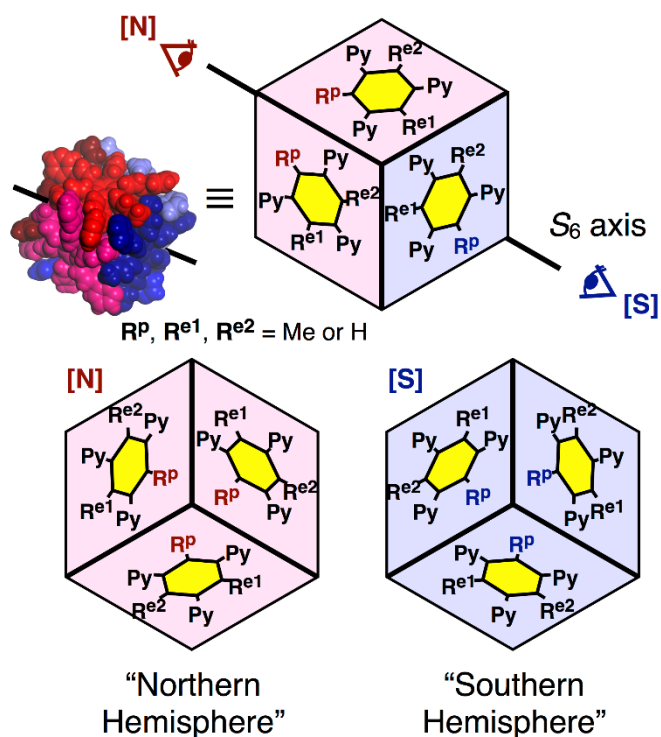


Figure 4-2. Schematic illustration of nanocube **9₆**; R^p denotes “polar” substituent, whereas R^{e1} and R^{e2} are “equatorial” substituents.

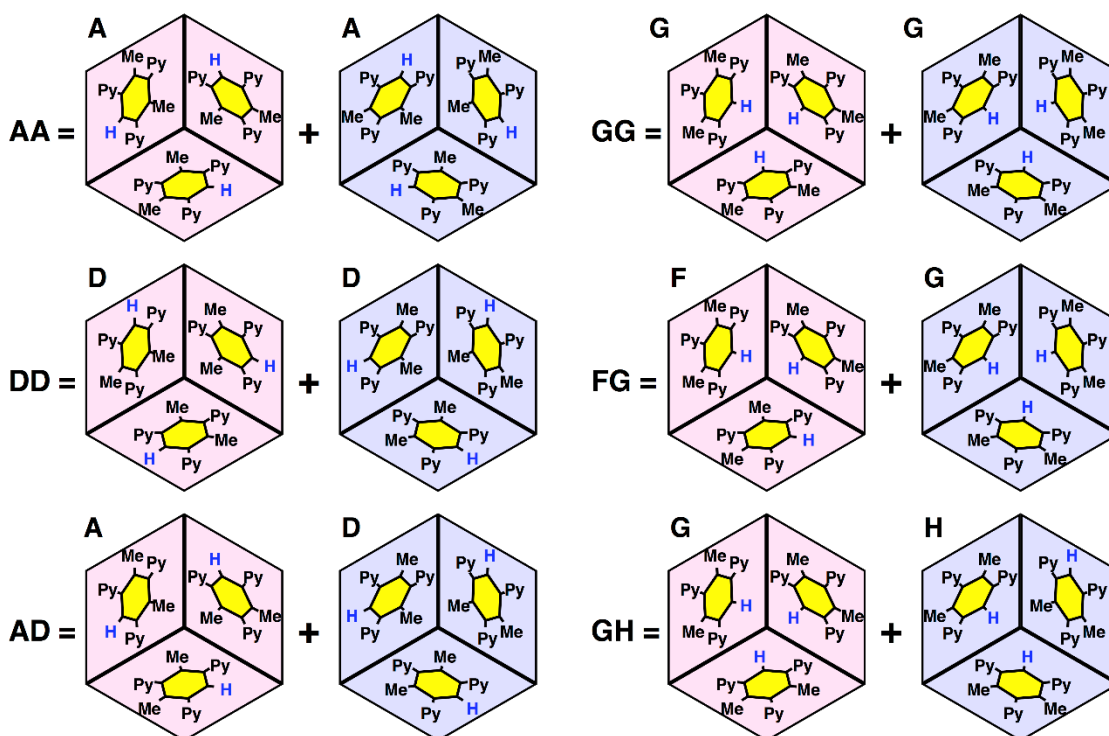


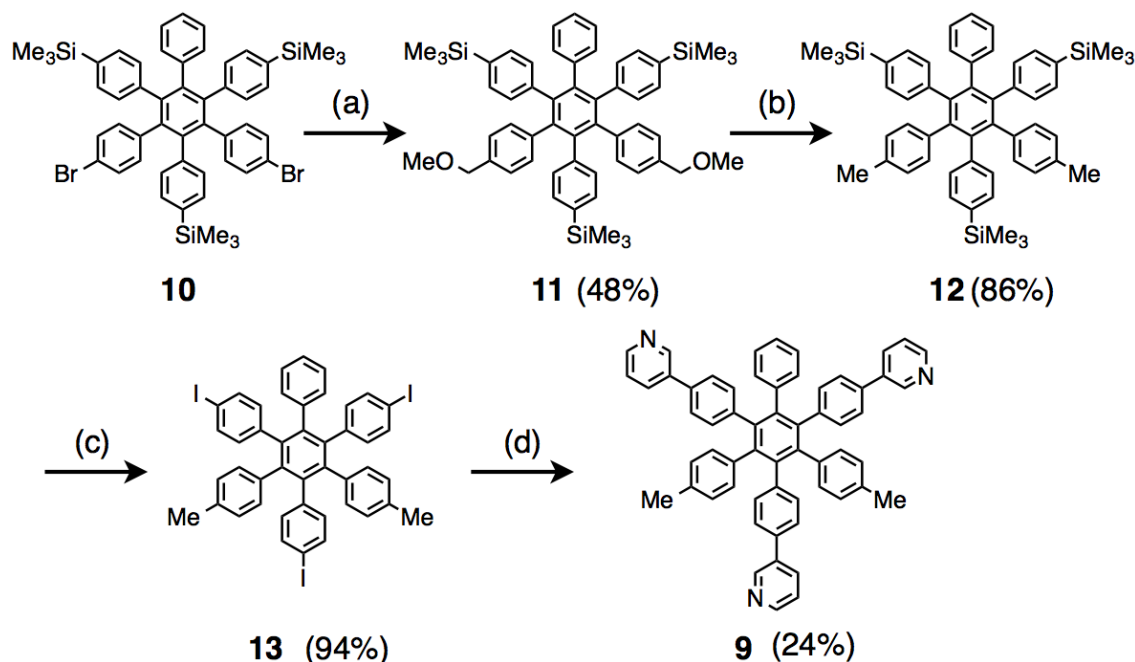
Figure 4-3. Schematic illustration of selected six isomers of nanocube **9₆**.

4.3. Results and discussions

4.3.1. Synthesis of the monomer molecule

A gear-shaped amphiphile **9** was prepared with a C_{2v} -symmetric hexaphenylbenzene (HPB) derivative **10** as a precursor (Scheme 4-1). Although the selective construction of the C_{2v} -symmetric substitution pattern on the HPB like compound **10** was impossible with conventional protocols,^[9] compound **10** is now selectively available through selective alternate trilithiation of brominated HPB derivatives, which was recently developed in the Hiraoka group.^[10,11] After dilithiation of compound **10**, direct introduction of the methyl groups was attempted with iodomethane at first. However, a partial protonation of the lithiated moieties was implied and it was very difficult to discriminate and separate the methylated compounds and protonated compounds because of their similar polarity. Methoxymethyl (MeOCH_2) groups were thus introduced as a polar equivalent of methyl groups to avoid the ambiguity of the number of methyl groups in the amphiphile. During the introduction of the MeOCH_2 groups, a larger amount of protonation was observed but compound **11** with two MeOCH_2 groups was unambiguously isolated in a moderate yield from the compounds with no or one MeOCH_2

group, which afforded separated spots on TLC. The MeOCH₂ groups in compound **11** were cleanly converted to methyl groups through reduction with LiNaph.^[12] Iododesilylation and Suzuki-Miyaura cross-coupling^[13] reactions of compound **12** afforded amphiphile **9**.



Scheme 4-1. Preparation of **9**. (a) *t*-BuLi (4.5 eq.), CH₃OCH₂Cl (4 eq.), THF, −78 °C; (b) lithium naphthalenide, THF, −43 °C; (c) ICl (3.3 eq.), CH₂Cl₂, −78 °C then rt; (d) 3-pyridylboronic acid (4.5 eq.), Pd₂(dba)₄ (5 mol%), PCy₃·HBF₄ (24 mol%), K₂CO₃ (4.5 eq.), dioxane/H₂O, 100 °C

4.3.2. NMR measurements: titration experiments

The association behavior of **9** was monitored by ¹H NMR (Figure 4-4). Amphiphile **9** existed as a monomer in CD₃OD at room temperature. Titration of D₂O into this solution resulted in the emergence of new peaks in the NMR spectrum. From the chemical shifts of the new peaks and the structural similarity of **9** to **1**, these peaks were assigned to nanocube **9**₆. Because the intensities of these peaks increased as the addition of D₂O, this association phenomenon should be driven by the hydrophobic effect. These peaks were broad, suggesting the possibility of the existence of many isomers of **9**₆. Considering these isomers **9**₆ as one species, the ratio of **9** and **9**₆ and the association constant *K*_a was calculated based on the peak intensities of the methyl groups in monomer and hexamers. The association constant of **9**₆ was roughly estimated to be *K*_a = 7 × 10¹⁵ M^{−5} at room temperature in the mixed solvent of CD₃OD / D₂O (v/v = 3/1), while

that of **1**₆ is $K_a = 3.2 \times 10^{-5}$ M⁻⁵ at room temperature in the same solvent.^[7] This result suggests the very lower tendency of formation of **9**₆ than that of **1**₆.

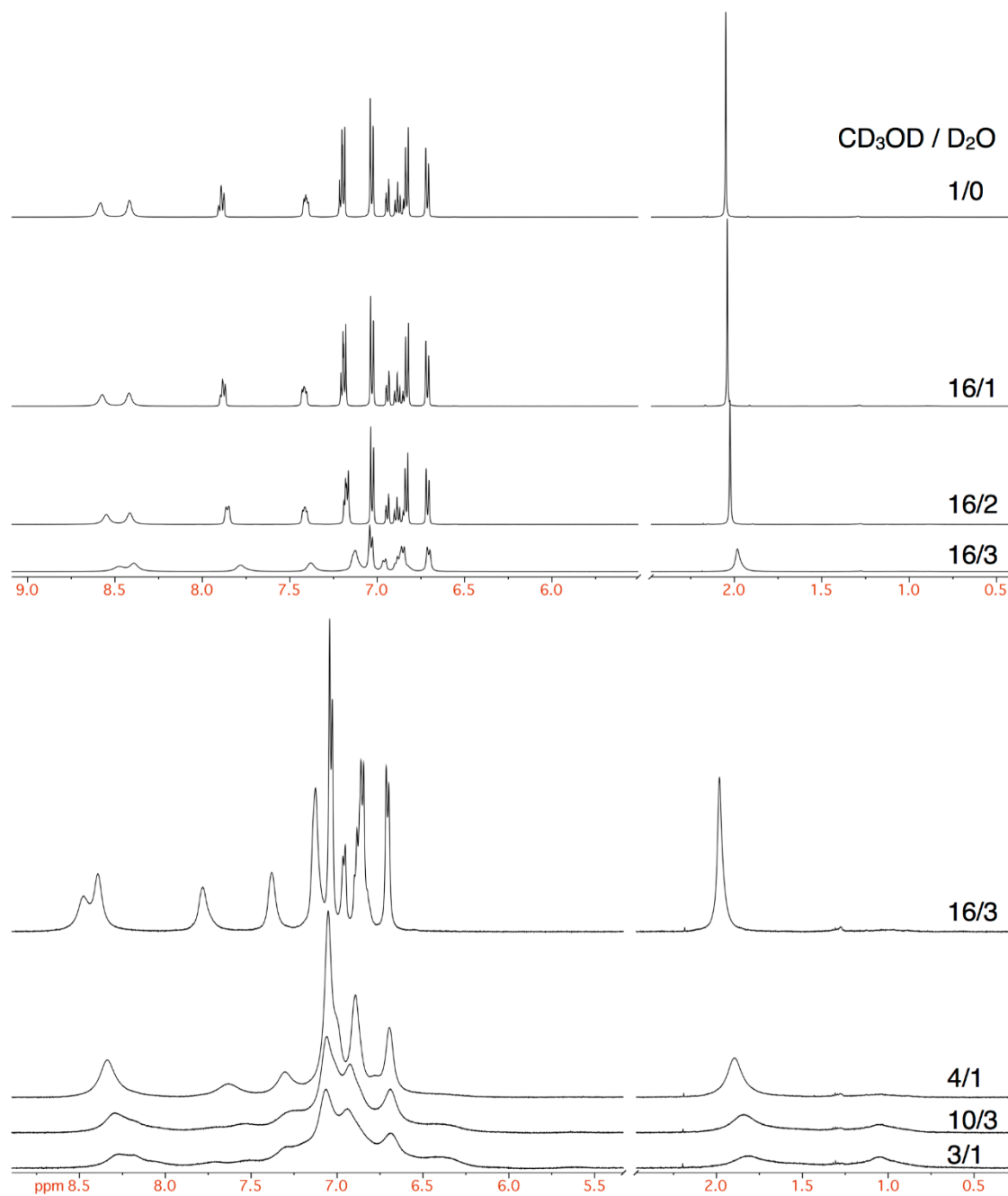


Figure 4-4. ¹H NMR spectra of **9**₆ in different ratios of CD₃OD/D₂O. The left side shows an aromatic region and the right side shows an aliphatic region.

4.3.3. NMR measurements: DOSY experiments

To confirm the formation of the nanocube **9₆**, the ¹H DOSY NMR spectrum of **9** in the mixed solvent of CD₃OD / D₂O (v/v = 3/1) was measured (Figure 4-5(a)). The diffusion coefficient of the species corresponding to the new peaks at 1.3 ppm was $1.33 \times 10^{-10} \text{ m}^2 \text{ s}^{-1}$. This value is comparable to that of **1₆** ($1.2 \times 10^{-10} \text{ m}^2 \text{ s}^{-1}$),^[6] indicating that the size of the species is close to that of **1₆**. This coincidence strongly suggests the existence of nanocube **9₆**. The diffusion coefficient of the species corresponding to the peak at 2.0 ppm was $2.05 \times 10^{-10} \text{ m}^2 \text{ s}^{-1}$. In view of Figure 4-4, this peak can be considered as the broadened and shifted peak of the methyl groups of the monomer **9**. To confirm this assignment, ¹H DOSY NMR spectrum of **2'**, a partially deuterated analog of **2**, was obtained (Figure 4-5(b)).^[14] As noted in 1.4.2, **2** does not aggregate in a mixed solvent of methanol/water, indicating that **2'** exists as monomer in this DOSY NMR measurement. The diffusion coefficient of **2'** was $2.05 \times 10^{-10} \text{ m}^2 \text{ s}^{-1}$, almost the same value as that of the species of 2.0 ppm. This coincidence indicates that this species has the same size as **2'** and hence is the monomer **9**.

4.3.4. NMR measurements: variable temperature experiments

To further compare the association behaviors of **1₆** and **9₆**, the temperature dependence of the formation constant of **9₆** in the mixed solvent of CD₃OD / D₂O (v/v = 4/1)^[15] was monitored by ¹H VT-NMR (Figure 4-6). At a lower temperature, new broad peaks assignable to **9₆** emerged. This fact indicates that the association reaction of **9** is encouraged at a lower temperature, that is, enthalpically favored, similarly to **1**. The shape of the emerged peaks in the upfield region (0.8-1.8 ppm) was very complicated, suggesting the coexistence of isomers of **9₆**.

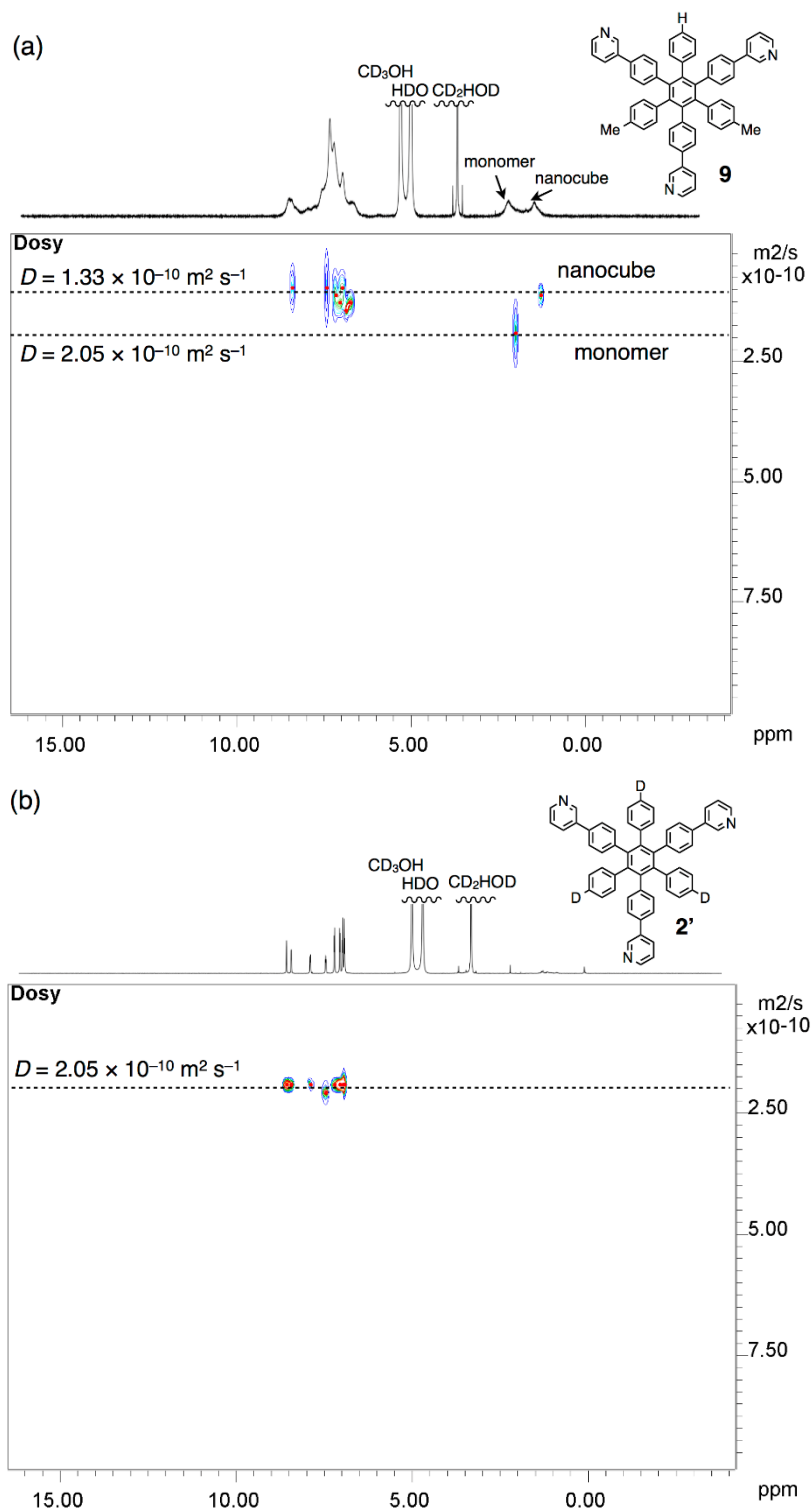


Figure 4-5. ¹H DOSY NMR spectrum of (a) **9**₆ and (b) **2'** (D₂O/CD₃OD = 1/3 (v/v), 298 K). The letters *D* indicate the diffusion coefficients of the corresponding species.

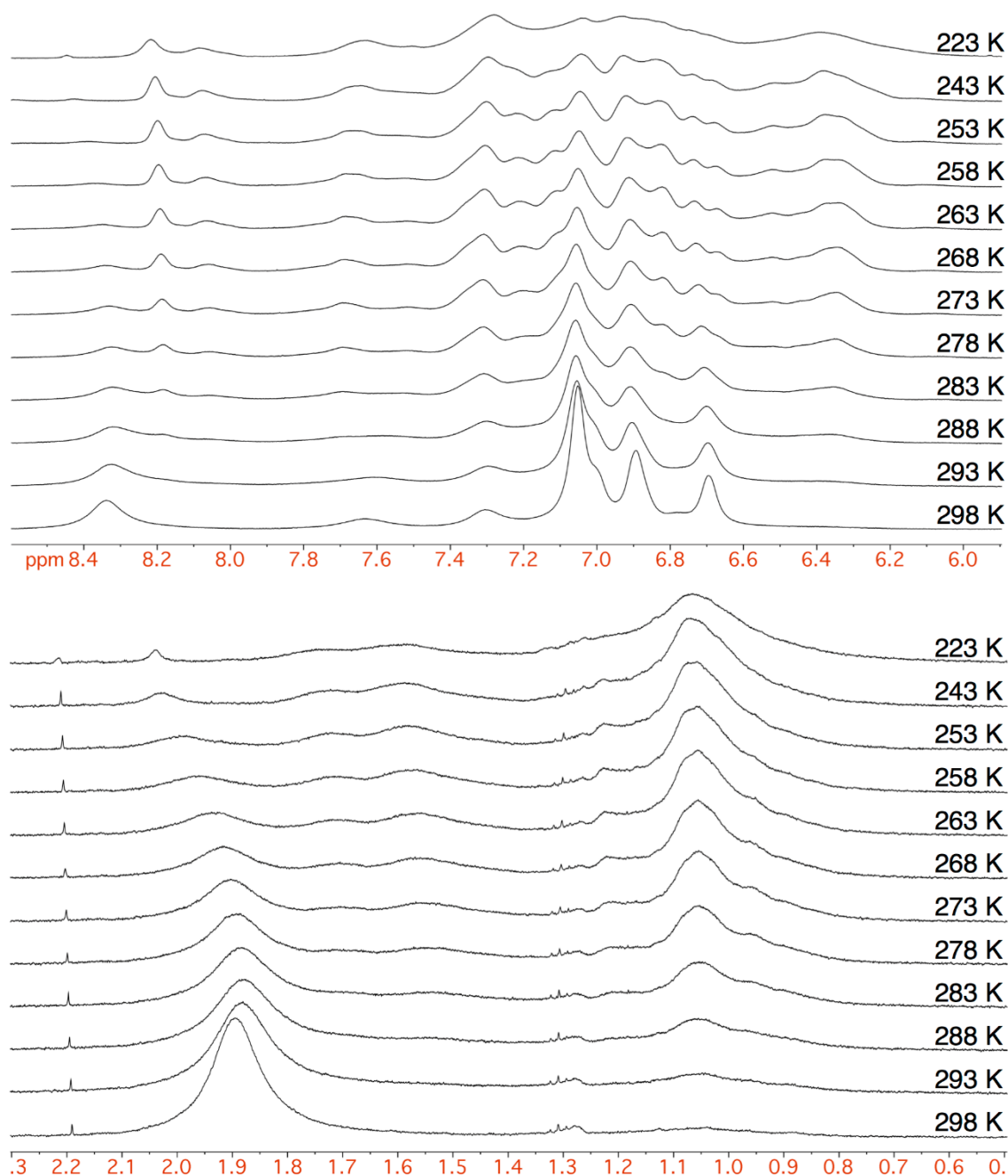


Figure 4-6. ^1H VT-NMR spectra of $\mathbf{9}_6$ in $\text{CD}_3\text{OD}/\text{D}_2\text{O}$ ($v/v = 4/1$). The upper figure shows an aromatic region and the lower figure shows an aliphatic region.

4.3.5. Isothermal titration calorimetry

To further investigate the thermodynamic property of the association of $\mathbf{9}$, isothermal titration calorimetry (ITC) measurement was conducted (Figure 4-7), according to the procedure in the case of $\mathbf{1}_6$.^[7] The obtained parameters for the association reaction of $\mathbf{9}$ into $\mathbf{9}_6$ in the mixed

solvent of CH₃OH / H₂O (v/v = 3/1) were $\Delta H^\circ = -43.6 \text{ kJ mol}^{-1}$ and $\Delta S^\circ = 170.6 \text{ J mol}^{-1} \text{ K}^{-1}$ at 296 K. These values indicate that the association of **9** is both enthalpically and entropically favored, in contrast to the association of **1**, which is entropically disfavored ($\Delta H^\circ = -216 \text{ kJ mol}^{-1}$ and $\Delta S^\circ = -354 \text{ J mol}^{-1} \text{ K}^{-1}$ at 293 K).^[7] This difference can be qualitatively explained by the tightness of the nanocube structures. As mentioned in 1.4.2, each monomer molecule constrains the motion of other monomers in the nanocubes, reducing the degree of freedom and the entropy of the systems. This effect is strong especially in tightly associated structures. The nanocube **1**₆ should be tighter than **9**₆. As a result, the entropic cost of the association of **9** can be reduced compared to that of **1**. The reduced entropic cost can be overcome by the contribution of the classical hydrophobic effect and result in the positive ΔS° value. The smaller ΔH° value of **9** than that of **1** can be explained by smaller vdW force. The smaller vdW force may result from the looser contact surface than **1**, which can be seen later in 4.3.7.

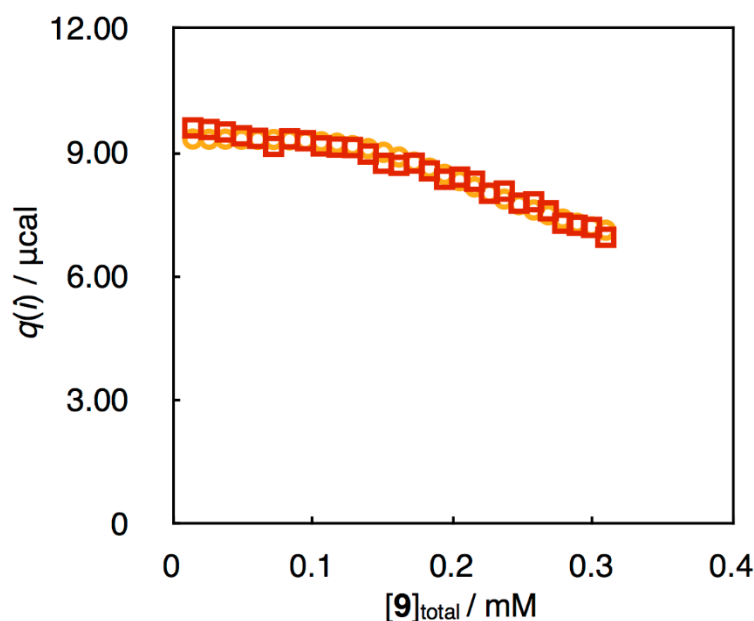


Figure 4-7. Plots of the integrated heat $q(i)$ measured by ITC for each injection of a solution of **9**₆ ($[\mathbf{9}] = 2.41 \text{ mM}$) to CH₃OH/H₂O (v/v = 3/1) in the cell, with respect to the total concentration of **9** in the cell, $[\mathbf{9}]_{\text{total}}$. Red open squares and orange open circles are experimental and calculated values, respectively.

4.3.6. MM calculation: optimized structures and their energies

Optimized structures of the abovementioned six isomers of **9**₆ were obtained by MM calculations. In the calculations, the initial structures were constructed by replacing the corresponding methyl groups of the crystal structure of **1**₆ with hydrogen atoms. The energy

values obtained from the calculations (Table 4-1) show that **GG**, **FG**, and **GH** are more stable by ~ 10 kcal mol⁻¹ than **AA**, **DD**, and **AD**, suggesting the formation of the former isomers in the experiments. This energetic difference is contributed positively by vdW forces and electrostatic interactions and negatively by dihedral angles. This difference suggests that **GG**, **FG**, and **GH** are more distorted than **AA**, **DD**, and **AD** so that they obtain larger intermolecular interaction at the cost of the distortion energies arising from dihedral angles. The formation energies of **GG**, **FG**, and **GH** are relatively similar, differing by only 1 kcal mol⁻¹. This value is comparable with the thermal energy of room temperature. This result suggests that **GG**, **FG**, **GH**, and similar isomers form as mixture in the association, consistent with the emergence of the very broad peaks in NMR measurements.

Table 4-1. Calculated energies (kcal mol⁻¹) of the six isomers of **9₆** based on MM calculation.

	total	bond	angle	dihedral	vdW	Coulomb	1-4 vdW	1-4 Coulomb
AA	897.95	56.09	43.49	746.76	-140.34	7.37	321.28	-136.72
DD	895.90	56.27	44.44	741.81	-137.68	6.62	321.22	-136.78
AD	896.32	56.19	44.03	744.25	-139.66	7.02	321.25	-136.76
GG	887.11	55.62	43.69	751.19	-151.90	3.92	321.34	-136.73
FG	888.40	55.66	43.61	750.95	-150.81	4.38	321.35	-136.73
HG	888.13	55.67	43.75	750.37	-150.49	4.21	321.35	-136.74

4.3.7. SAVPR analysis: intersurface distance distributions

To investigate further the difference of the stability of the isomers, their calculated structures were analyzed by the SAVPR method (Figure 4-8). While the intersurface distance distributions of **GG**, **FG**, and **GH** are similar and those of **AA**, **DD**, and **AD** are also similar, **GG** possesses much larger contact surface of short intersurface distance (< 2 Å) than **AA**. This difference of intersurface distance distribution will affect the intermolecular interaction in the isomers and their stabilities. This result is consistent with the suggestion from MM calculation that **GG**, **FG**, and **GH** are more stabilized than **AA**, **DD**, and **AD** by their vdW forces. The contact surface of short intersurface distance in **GG** is also larger than in **2₆**. This observation is consistent with the result that **2** does not aggregate at all in the same condition. When **GG** and **1₆** are compared,

their contact surfaces of short intersurface distance are similar while that of large intersurface distance (~ 2 Å) in **GG** is smaller than in **1₆**. This difference explains the difference of the association constants of **1₆** and **9₆**.

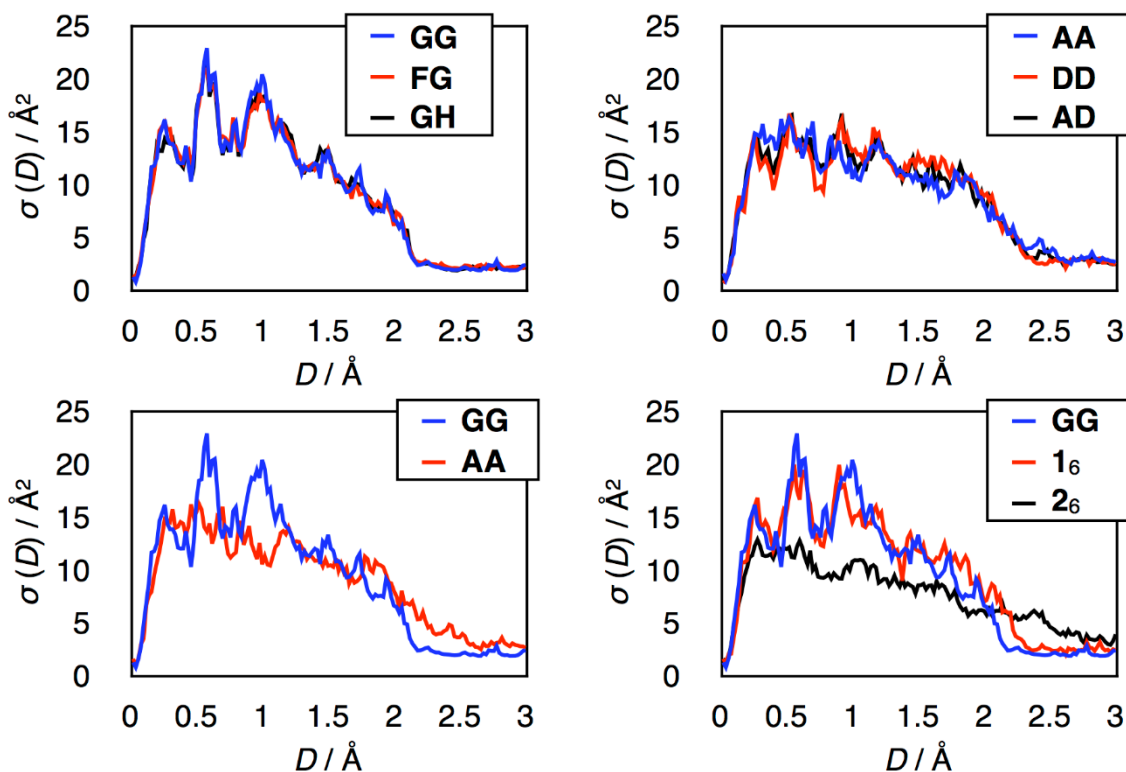


Figure 4-8. Intersurface distance distributions of the nanocubes **1₆**, **2₆**, and selected isomers of **9₆** calculated by the SAVPR method; the structure of **1₆** and **2₆** were calculated in Chapter 3.

4.4. Conclusions

In this chapter, the effect of one methyl group on the association behavior of nanocubes was investigated. Instead of the formation of an unambiguous and unique product, a mixture of some isomers of **9₆** was obtained from the association of **9**. The formation of such a mixture was supported from MM calculation and the SAVPR method. The association behavior of **9** was different from that of **1** and **2**. This difference should be an important example demonstrating that only one methyl group largely affects the intermolecular interactions and the self-assembly behavior.

4.5. Experimental procedures

General information

^1H NMR and ^{13}C NMR spectra were recorded using a Bruker AV-500 (500 MHz) spectrometer. All ^1H spectra were referenced using residual solvent peaks. High-resolution mass spectra (HRMS) were obtained using a Waters Xevo G2 ToF mass spectrometer. Melting points were determined using a SCINICS SMP-300 instrument. Silica-gel column chromatography was carried out with Merck Silica gel 60 (0.040–0.063 mm) otherwise noted.

Materials

Unless otherwise noted, all solvents and reagents were obtained from commercial suppliers (TCI Co., Ltd., WAKO Pure Chemical Industries Ltd., KANTO Chemical Co., Inc., and Sigma-Aldrich Co.) and were used as received. Compound **10**^[11] was prepared according to the literature.

Preparation of compound 9

To the solution of compound **10** (0.450 g, 0.495 mmol) in THF (9 mL) was added the pentane solution of *t*-BuLi (1.43 M, 1.56 mL, 2.23 mmol) at $-78\text{ }^\circ\text{C}$. The solution was stirred for 15 min at $-78\text{ }^\circ\text{C}$. To the mixture was added chloromethyl methyl ether (0.151 mL, 1.98 mmol). After the removal of the cooling bath, the mixture was stirred for 1 h and then the volatile was removed in vacuo. Silica-gel column chromatography (Et_2O /Hexane = 1/30 to 1/15) of the residue afforded compound **11** (0.198 g, 48%) as a colorless solid.

11: m.p. 200–201 $^\circ\text{C}$; ^1H NMR (500 MHz, C_6D_6 , 298 K): δ 7.18–7.14 (m, 8H), 7.12 (d, J = 8.0 Hz, 4H), 7.08 (d, J = 8.0 Hz, 4H), 7.07 (d, J = 8.0 Hz, 2H), 6.82 (d, J = 8.0 Hz, 4H), 6.79 (t, J = 7.5 Hz, 2H), 6.66 (t, J = 7.5 Hz, 1H), 3.91 (s, 4H), 2.93 (s, 6H), 0.02 (s, 18H), 0.01 (s, 9H); $^{13}\text{C}\{^1\text{H}\}$ NMR (126 MHz, CDCl_3 , 298 K): δ 141.10, 140.56, 140.52, 140.48, 140.32, 140.16, 136.59, 134.44, 131.57, 130.86, 126.61, 126.48, 125.16, 74.40, 56.98, -1.07 (16 signals; seven signals in an aromatic region and one signal from TMS group were not observed because of overlapping.); HRMS (ASAP) Calcd for $[\text{M}]^+$ $\text{C}_{55}\text{H}_{62}\text{O}_2\text{Si}_3$ 838.4058, found 838.4058.

The mixture of granular lithium (20.6 mg, 2.96 mmol) and naphthalene (0.455 g, 3.55 mmol)

in THF (4 mL) was vigorously stirred for 4 h at rt to afford the black solution of lithium naphthalenide (LiNaph). To the solution of compound **11** (0.198 g, 0.236 mmol) in THF (2.5 mL) was added the LiNaph solution (2.6 mL; LiNaph 1.9 mmol) dropwise at $-43\text{ }^{\circ}\text{C}$. The solution was stirred for 40 min at $-43\text{ }^{\circ}\text{C}$ and quenched with MeOH (1 mL). After the addition of water, the aqueous layer was extracted with CHCl_3 (5 mL $\times 2$) and the combined extracts were dried over anhydrous MgSO_4 and filtered. Then the solvent was removed in vacuo and silica-gel column chromatography (Hex to AcOEt/Hex = 1/50) afforded compound **12** (0.159 g, 86%) as a colorless solid.

12: m.p. $>300\text{ }^{\circ}\text{C}$; ^1H NMR (500 MHz, CDCl_3 , 298 K): δ 6.98 (d, $J = 8.0\text{ Hz}$, 2H), 6.97 (d, $J = 8.0\text{ Hz}$, 4H), 6.83–6.74 (m, 11H), 6.64 (d, $J = 8.0\text{ Hz}$, 4H), 6.61 (d, $J = 8.0\text{ Hz}$, 4H), 2.08 (s, 6H), 0.10 (s, 9H), 0.09 (s, 18H); $^{13}\text{C}\{^1\text{H}\}$ NMR (126 MHz, CDCl_3 , 298 K): δ 141.51, 141.39, 140.87, 140.70, 140.41, 140.36, 140.30, 137.70, 136.42, 136.35, 134.26, 131.64, 131.52, 131.47, 130.93, 127.26, 126.54, 125.01, 21.1, -1.02 , -1.03 (21 signals; two signals in an aromatic region were not observed because of overlapping.); HRMS (ASAP) Calcd for $[\text{M}]^+ \text{C}_{53}\text{H}_{58}\text{Si}_3$ 778.3846, found 778.3846.

To the solution of compound **12** (0.145 g, 0.186 mmol) in CH_2Cl_2 (2 mL) was added the solution of ICl in CH_2Cl_2 (1.0 M, 0.61 mL, 0.61 mmol) at $-78\text{ }^{\circ}\text{C}$. After the removal of the cooling bath, the mixture was stirred for 30 min and then quenched with sat. Na_2SO_3 . The aqueous layer was extracted with CH_2Cl_2 (10 mL $\times 2$) and the combined extracts were dried over anhydrous MgSO_4 and filtered. Then the solvent was removed in vacuo to afford compound **13** (0.164 g, 94%) as a colorless solid. This product was pure enough and used without further purification for the next reaction.

13: ^1H NMR (500 MHz, CDCl_3 , 298 K) δ 7.18 (d, $J = 8.5\text{ Hz}$, 2H), 7.17 (d, $J = 8.5\text{ Hz}$, 4H), 6.92–6.86 (m, 3H), 6.76–6.71 (m, 2H), 6.70 (d, $J = 7.8\text{ Hz}$, 4H), 6.61 (d, $J = 7.8\text{ Hz}$, 4H), 6.52 (d, $J = 8.5\text{ Hz}$, 2H), 6.51 (d, $J = 8.5\text{ Hz}$, 4H), 2.15 (s, 6H); ^{13}C NMR (126 MHz, CDCl_3 , 298 K) δ 140.46, 140.31, 140.23, 140.04, 139.73, 139.44, 136.78, 135.88, 135.28, 133.30, 131.29, 131.10, 127.94, 127.15, 125.82, 91.29, 21.28 (17 signals; four signals in an aromatic region were not observed because of overlapping.); HRMS (ASAP) m/z : exact mass $[\text{M}]^+ 939.9561$, $\text{C}_{44}\text{H}_{31}\text{I}_3$ requires 939.9560.

The suspension of **13** (0.164 g, 0.174 mmol), 3-pyridylboronic acid (96.5 mg, 0.785 mmol), Pd₂(dba)₃ (8.0 mg, 8.7 μmol), PCy₃·HBF₄ (15.4 mg, 42 μmol), and K₂CO₃ (0.166 g, 0.783 mmol) in dioxane (2 mL) and water (1 mL) was stirred for 2 h at 100 °C. After the addition of water, the aqueous layer was extracted with CHCl₃ (5 mL ×3) and the combined extracts were dried over anhydrous MgSO₄ and filtered. Then the solvent was removed in vacuo and silica-gel column chromatography (Wakogel® 50NH₂ AcOEt/Hex = 1/2) followed by recrystallization from MeCN afforded compound **9** (33 mg, 24%) as a pale yellow solid.

9: m.p. >300 °C; ¹H NMR (500 MHz, CDCl₃, 298 K) δ 8.71 (dd, *J* = 2.3, 0.6 Hz, 1H), 8.69 (dd, *J* = 2.3, 0.6 Hz, 2H), 8.50–8.48 (m, 3H), 7.76–7.71 (m, 3H), 7.28–7.24 (m, 3H), 7.15 (d, *J* = 8.4 Hz, 2H), 7.14 (d, *J* = 8.4 Hz, 4H), 6.94 (d, *J* = 8.4 Hz, 2H), 6.94 (d, *J* = 8.4 Hz, 4H), 6.90–6.84 (m, 5H), 6.75 (d, *J* = 8.0 Hz, 4H), 6.68 (d, *J* = 8.0 Hz, 4H), 2.09 (s, 6H); ¹³C NMR (126 MHz, CDCl₃, 298 K) δ 148.21, 148.17, 141.02, 140.93, 140.68, 140.57, 140.23, 139.95, 137.33, 136.38, 136.33, 134.96, 134.25, 134.18, 134.01, 132.27, 131.51, 131.33, 127.76, 126.98, 125.56, 125.29, 123.47, 21.20 (24 signals; seven signals in an aromatic region were not observed because of overlapping); HRMS (ASAP) *m/z*: exact mass [M]⁺ 793.3459, C₅₉H₄₃N₃ requires 793.3457.

Monitor of self-assembly of **9** by NMR measurement

Amphiphile **9** (0.89 mg) was dissolved in CD₃OD (550 μL). Into this sample, D₂O was titrated and the self-assembly was monitored by ¹H NMR. At the point of v/v = 4/1, the self-assembly was monitored at several temperatures.

Isothermal titration calorimetry measurement

Dilution isothermal titration calorimetry (ITC) experiments were conducted on a Malvern MicroCal iTC₂₀₀. The calorimetric cell was filled with a 1:3 mixed solvent of H₂O and CH₃OH (0.2047 mL). Before ITC experiment, the concentration of the nanocube in H₂O/CH₃OH solution was determined by ¹H NMR measurement with acetanilide as an internal standard. For one titration experiment, totally 29 injections were performed and in each injection 1 μL of aqueous solution of the nanocube was added except the first injection, 0.2 μL, which was

discarded in the experiment. An interval time of 150 s between each injection was applied to enable equilibration. According to the case of **1**,^[7] the data set was analyzed by the modified Wittung-Stafshede's method^[16] to determine the dissociation constant, the dissociation enthalpy, and the heat of dilution.

Molecular mechanics calculation

The structures of nanocubes (**1**₆, **2**₆, and six isomers of **9**₆) were optimized and their energies were evaluated by the general AMBER force field (GAFF) in AMBER 9 program package. The structures of the monomers were generated by the dissociation of nanocubes in Materials Studio software (version 8.0; Biovia Inc., USA). Estimations of surface areas and intersurface distance distributions were conducted following the procedure mentioned in Chapter 3.

Counting the isomers of nanocube **9**₆

Here the author explains that the nanocube **9**₆ has 138 geometrical isomers. The nanocube **9**₆ consists of the “northern hemisphere” and the “southern hemisphere”. Both of “hemispheres” have 11 isomers (**A**, **B**, ..., **K**; Figure 4-9), where three of them are *C*₃-symmetric and the others are *C*₁-symmetric. Each isomer of the nanocube is expressed with a combination of the isomers of the hemispheres. Hereafter, the combinations of the hemispheres are expressed with two isomer labels, where the first letter denotes the northern hemisphere and the second letter denotes the southern hemisphere. For example, one of the combinations is **AB**, whose northern hemisphere is isomer **A** and southern hemisphere is isomer **B**. This combination **AB** is the enantiomer of **BA**. When such enantiomers are not discriminated, the number of the combinations of two hemispheres is $11 + 11 \times 10 / 2 = 66$. If both of hemispheres possess *C*₁ symmetry, there are three different relative orientations to combine them and the combination corresponds to three isomers of **9**₆. For example, **BC** has three isomers of the nanocube (and each of them is the enantiomer of one of the three isomers of **CB**). Because eight isomers of the hemisphere **A–K** are *C*₁-symmetric, this situation corresponds to $8 + 8 \times 7 / 2 = 36$ combinations of hemispheres, generating $3 \times 36 = 108$ isomers of the nanocube. The number of the other combinations, which include at least one isomer of hemispheres with *C*₃ symmetry, is $66 - 36 = 30$. This symmetry removes the difference of the relative orientation of the hemispheres,

resulting in only one isomer for each combination. For example, **AA** and **AB** have only one isomer of the nanocube. By that, 30 combinations and 30 isomers belong to this situation. Therefore, $108 + 30 = 138$ isomers of **9₆** exist.

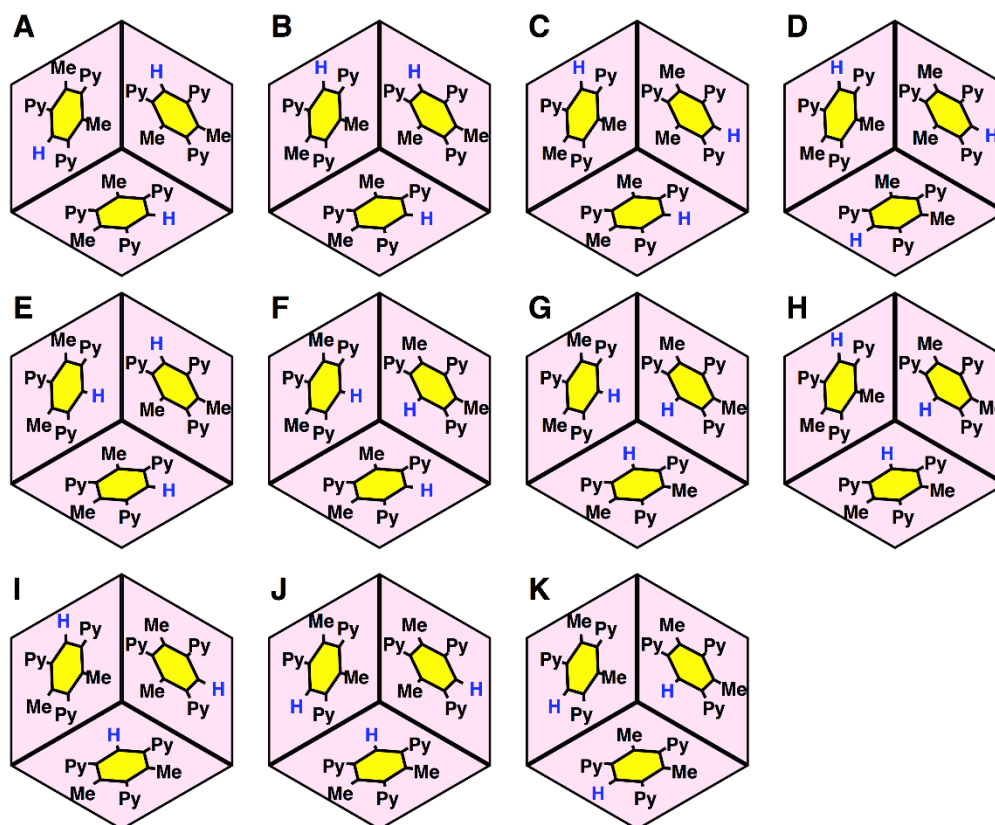


Figure 4-9. Schematic illustration of eleven isomers of “northern hemisphere” of nanocube **9₆**. The same letters also denote the corresponding “southern hemispheres”, which are the enantiomers of “northern hemispheres”. In these isomers, **A**, **D**, and **G** are C_3 -symmetric, whereas the others are C_1 -symmetric.

References and Notes

- ¹ a) Tanford, C. *Science* **1978**, *200*, 1012–1018; b) Tanford, C. *The Hydrophobic Effect: Formation of Micelles and Biological Membranes*, Wiley, New York, 1973; c) Levy, Y.; Onuchic, J. N. *Annu. Rev. Biophys. Biomol. Struct.* **2006**, *35*, 389–415; d) Snyder, P. W.; Lockett, M. R.; Moustakas, D. T.; Whitesides, G. M. *Eur. Phys. J. Special Topics* **2014**, *223*, 853–891; e) Baldwin, R. L. *J. Mol. Biol.* **2007**, *371*, 283–301.
- ² a) Jordan, J. H.; Gibb, B. C. *Chem. Soc. Rev.* **2015**, *44*, 547–585; b) Laughrey, Z.; Gibb, B. C. *Chem. Soc. Rev.* **2011**, *40*, 363–386; c) Biro, S. M.; Rebek, J. Jr. *Chem. Soc. Rev.* **2007**, *36*, 93–104; d) Oshovsky, G. V.; Reinhoudt, D. N.; Verboom, W. *Angew. Chem., Int. Ed.* **2007**, *46*, 2366–2393; e) Krieg, E.; Bastings, M. M. C.; Besenius, P.; Rybtchinski, B. *Chem. Rev.* **2016**,

- 116, 2414–2477; f) Tahara, K.; Lei, S.; Adisoejoso, J.; De Feyter, S.; Tobe, Y. *Chem. Commun.* **2010**, 46, 8507–8525.
- ³ Zhang, W.; Laursen, R. A. *J. Biol. Chem.* **1998**, 273, 34806–34812.
- ⁴ St George-Hyslop, P. H. *Biol. Psychiatry* **2000**, 47, 183–199.
- ⁵ a) Gibb, C. L. D.; Gibb, B. C. *Chem. Commun.* **2007**, 1635–1637; b) Hooley, R. J.; Van Anda, H. J.; Rebek, J. Jr. *J. Am. Chem. Soc.* **2007**, 129, 13464–13473; c) Yazaki, K.; Sei, Y.; Akita, M.; Yoshizawa, M. *Nat. Commun.* **2014**, 5, 5179; d) Ogoshi, T.; Demachi, K.; Kitajima, K.; Yamagishi, T. *Chem. Commun.* **2011**, 47, 10290–10292; e) Liu, S.; Gan, H.; Hermann, A. T.; Rick, S. W.; Gibb, B. C. *Nat. Chem.* **2010**, 2, 847–852; f) Jiang, W.; Ajami, D.; Rebek, J. Jr. *J. Am. Chem. Soc.* **2012**, 134, 8070–8073.
- ⁶ Hiraoka, S.; Harano, K.; Shiro, M.; Shionoya, M. *J. Am. Chem. Soc.* **2008**, 130, 14368–14369.
- ⁷ Hiraoka, S.; Harano, K.; Nakamura, T.; Shiro, M.; Shionoya, M. *Angew. Chem., Int. Ed.* **2009**, 48, 7006–7009.
- ⁸ Hiraoka, S.; Nakamura, T.; Shiro, M.; Shionoya, M. *J. Am. Chem. Soc.* **2010**, 132, 13223–13225.
- ⁹ Feng, X.; Pisula, W.; Müllen, K. *Pure. Appl. Chem.* **2009**, 81, 2203–2224.
- ¹⁰ Kojima, T.; Hiraoka, S. *Org. Lett.* **2014**, 16, 1024–1027.
- ¹¹ Kojima, T.; Hiraoka, S. *Chem. Commun.* **2014**, 50, 10420–10423.
- ¹² Liu, H.-J.; Yip, J.; Shia, K.-S. *Tetrahedron Lett.* **1997**, 38, 2253–2256.
- ¹³ Kudo, N.; Perseghini, M. Fu, G. C. *Angew. Chem., Int. Ed.* **2006**, 45, 1282–1284.
- ¹⁴ The synthesis of **2'** is easily achieved by simple modification of that of **1**. The synthetic detail is shown in: Tsujimoto, Y.; Kojima, T.; Hiraoka, S. *Chem. Sci.* **2014**, 5, 4167–4172. The deuteration simplifies the ¹H NMR spectrum, facilitating the analysis.
- ¹⁵ Unfortunately, the same ratio of mixed solvent as **1**₆, CD₃OD / D₂O (v/v = 3/1), was not applicable because of precipitation of **9**.
- ¹⁶ Luke, K.; Apiyo, D.; Wittund-Stafshede, P. *Biophys. J.* **2005**, 89, 3332–3336.

Chapter 5.

General Conclusion and Prospects

5.1. General conclusion

This thesis described the development of a semiquantitative method, SAVPR, to evaluate the complementarity between molecular surfaces in supramolecular complexes. This method efficiently evaluates and visualizes the intersurface distance distribution of a given structure. Because intersurface distance has very large influence on the strength of intermolecular interaction, this distribution enables semiquantitative estimation of association constant of a given supramolecular structure.

In Chapter 1, the importance of intermolecular interactions was explained. Intermolecular interactions drive many interesting phenomena. The knowledge and literature studies on intermolecular interactions were also given. Finally, the challenge in quantitatively understanding them was pointed out.

In Chapter 2, the SAVPR method, a novel method to evaluate and visualize intersurface distance distribution, was introduced. In the chapter, the concept and the formulation of the method was described, along with the related fundamental knowledge about molecular surfaces.

In Chapter 3, the applicability and the versatility of the SAVPR method were demonstrated. This method succeeded in explaining the large difference of association constants of nanocubes semiquantitatively. The SAVPR method was also applied to some host-guest systems. As a result, the deviation of the association constant from its correlation with contact surface area was explained. These results emphasize not only the usefulness of the SAVPR method but also the importance of a detailed structure of contact surface, especially, intersurface distance distribution.

In Chapter 4, an example of application of SAVPR was introduced. The association behavior of **9** was described. The SAVPR method explained the order of the association constants of **1**₆,

2₆, and **9**₆. The resulted complex spectrum was assigned to the mixture of isomers of **9**₆. By means of SAVPR and MM calculation, several species can be the most stable among the isomers, consistent with the production of the mixture.

5.2. Prospects

Comprehensive knowledge on intermolecular interactions should be a fundamental key to future sciences. For instance, development of supramolecular structures, molecular machines, and medicines will be encouraged by the knowledge. Such knowledge is also required for deeper understanding of biologic systems and other complex systems. In the practical context of these applications, simple and quantitative methods to predict the intensity of intermolecular interaction will be needed. SAVPR is an attempt to develop such a method. This study, understanding of intermolecular interactions and development of a method to evaluate them, will contribute to culture and civilization by understanding the nature and applying the knowledge.

Acknowledgements

The studies in this thesis were conducted in the Hiraoka laboratory in the University of Tokyo. The author expresses sincerest acknowledgement to the members of the laboratory, especially to:

Professor Shuichi Hiraoka, for recruiting me to the laboratory and providing stimulating environments and fascinating and challenging themes.

Dr. Tatsuo Kojima, for providing many technical and mental supports, fruitful discussions and suggestions, and comfortable environment for research.

In the computational studies, many data and suggestions were provided from the Tachikawa laboratory in Yokohama City University. The author expresses deep thanks to Professor Masanori Tachikawa, Dr. Takako Mashiko, and Dr. Umpei Nagashima.

The author thanks Ms. Etsuko Suzuki (Nihon Waters K.K.) for mass spectrometry measurements.

The technical knowledge on chemical research was cultivated in the master course of the author in the Kojima laboratory in the University of Tokyo. The author also expresses cordial gratitude to the members of the laboratory, especially to Professor Emeritus Norimichi Kojima and Dr. Atsushi Okazawa.

The author also expresses heartfelt appreciation to Professor Keiichiro Watanabe and Ms. Eri Kawase in the Division for Counseling and Support (Office for Mental Health Support and Communication Support Room) for the tender and long-term mental supports.

Finally, the author deeply appreciates the family, friends, and everything that has supported the author.

Naru Tanaka